Reconstructing human brown fat developmental trajectory *in vitro*

Graphical abstract

A single cell RNA sequencing census of developing mouse brown adipose tissue

E11.5 — E15.5

single cell RNA sequencing and in silico lineage analysis

pseudotime

Gata6 identifies a population of brown adipocyte precursors

in silico lineage analysis + Pax7 and Gata6 lineage tracing

E11.5 — E15.5

Pax3 → Pax7 → Pax7 → skeletal muscle

tendon — bone — smooth muscle

Fibro → Gata6 → brown adipocytes

Dermis — cartilage — connective tissue

Directed differentiation of human pluripotent stem cells towards brown adipocytes

OCT4/SOX2 → PAX3 → PDGFRA → GATA6 → UCP1

hiPSCs — dermomyotome — fibroblastic precursor — brown adipocyte precursor — Brown adipocyte

Highlights

- A single-cell RNA-sequencing census of developing mouse brown adipose tissue

- GATA6 identifies a population of brown adipocyte precursors

- Directed differentiation of human pluripotent stem cells toward brown adipocytes

Authors

Jyoti Rao, Yannis Djeffal, Jerome Chal, ..., Fiona M. Watt, Yu-Hua Tseng, Olivier Pourquié

Correspondence

pourquie@genetics.med.harvard.edu

In brief

Brown adipose tissue controls thermogenesis and regulates metabolism. Rao et al. use single-cell RNA sequencing to analyze its development in mouse embryos and recapitulate the developmental cues experienced by brown adipocytes *in vitro* to engineer a protocol to differentiate human pluripotent stem cells into functional brown adipocytes.

CellPress

Developmental Cell

CellPress

Resource

Reconstructing human brown fat developmental trajectory *in vitro*

Jyoti Rao,[1,2,3,10] Yannis Djeffal,[1,2,3] Jerome Chal,[1,2,3] Fabio Marchianò,[4] Chih-Hao Wang,[5,11] Ziad Al Tanoury,[1,2,3] Svetlana Gapon,[1,2,3] Alicia Mayeuf-Louchart,[6] Ian Glass,[7] Elizabeth M. Sefton,[8] Bianca Habermann,[4] Gabrielle Kardon,[8] Fiona M. Watt,[9] Yu-Hua Tseng,[5] and Olivier Pourquié[1,2,3,12,*]

[1]Department of Pathology, Brigham and Women's Hospital, 60 Fenwood Road, Boston, MA 02115, USA
[2]Department of Genetics, Harvard Medical School, 60 Fenwood Road, Boston, MA 02115, USA
[3]Harvard Stem Cell Institute, Harvard University, Cambridge, MA 02138, USA
[4]Aix-Marseille University, CNRS, IBDM, The Turing Center for Living Systems, 13009 Marseille, France
[5]Section on Integrative Physiology and Metabolism, Joslin Diabetes Center, Harvard Medical School, Boston, MA 02215, USA
[6]Univ. Lille, INSERM, CHU Lille, Institut Pasteur de Lille, 59000 Lille, France
[7]Department of Pediatrics, University of Washington School of Medicine, Seattle, WA 98195, USA
[8]Department of Human Genetics, University of Utah, Salt Lake City, UT 84112, USA
[9]King's College London Centre for Stem Cells and Regenerative Medicine, Great Maze Pond, London SE1 9RT, UK
[10]Present address: Institute of Human Biology, Roche Pharma Research and Early Development, Basel 4070, Switzerland
[11]Present address: Graduate Institute of Biomedical Sciences, China Medical University, Taichung 40402, Taiwan
[12]Lead contact
*Correspondence: pourquie@genetics.med.harvard.edu
https://doi.org/10.1016/j.devcel.2023.08.001

SUMMARY

Brown adipocytes (BAs) represent a specialized cell type that is able to uncouple nutrient catabolism from ATP generation to dissipate energy as heat. In humans, the brown fat tissue is composed of discrete depots found throughout the neck and trunk region. BAs originate from a precursor common to skeletal muscle, but their developmental trajectory remains poorly understood. Here, we used single-cell RNA sequencing to characterize the development of interscapular brown fat in mice. Our analysis identified a transient stage of BA differentiation characterized by the expression of the transcription factor GATA6. We show that recapitulating the sequence of signaling cues identified in mice can lead to efficient differentiation of BAs *in vitro* from human pluripotent stem cells. These precursors can in turn be efficiently converted into functional BAs that can respond to signals mimicking adrenergic stimuli by increasing their metabolism, resulting in heat production.

INTRODUCTION

In humans, brown adipose tissue (BAT) is present most abundantly in the interscapular region at birth and in the supraclavicular region in adulthood.[1–5] Brown adipocytes (BAs) derive from the paraxial mesoderm, an embryonic tissue that flanks the neural tube. In mammals, the paraxial mesoderm first forms through gastrulation in the primitive streak and generates the presomitic mesoderm (PSM) in the posterior region of the embryo. As it matures, the PSM forms epithelial somites that become organized in two parallel arrays of segments, providing the blueprint for the future metameric organization of vertebrae and other trunk derivatives. Soon after their formation, the ventral part of somites forms the mesenchymal sclerotome that yields the axial skeleton. The dorsal part of the somite remains epithelial, forming the dermomyotome. This compartment is composed of cells expressing the transcription factor Pax3, and it generates the dermis of the back and skeletal muscles of the body.

Lineage tracing experiments have shown that murine interscapular brown fat arises from Pax3, Meox1, and Myf5-expressing der-

momyotomal cells in the embryo.[6–9] During development, Pax3-positive dermomyotome cells give rise to multipotential progenitor cells expressing Engrailed1 and Pax7. These multipotent cells develop into dermal cells, skeletal muscle, and BAs.[10,11] Lineage tracing of Pax7 multipotent progenitors in mice shows that between E9.5 (embryonic day 9.5) and E11.5, these cells can give rise to skeletal muscle, dermis, and some BAs.[9,11] The contribution of Pax7 progenitors becomes restricted to the skeletal muscle lineage at E11.5–12.5. Overall, the hierarchy of somitic precursors giving rise to this tissue is still poorly characterized.[12]

Our knowledge of human BAT development is even more limited. Current *in vitro* models to study human BAT are mostly based on BAs differentiated *in vitro* from primary cell lines and stromal vascular cells.[13] Several protocols have also been established to differentiate human pluripotent stem cells (hPSCs) into BAs using either transgenic overexpression of transcription factors[14] or treatment with growth factors and small molecules.[15] Other reported methods rely on serum-based spontaneous differentiation or treatment of hPSCs with a cytokine cocktail.[16–18] Recently, protocols allowing the generation of
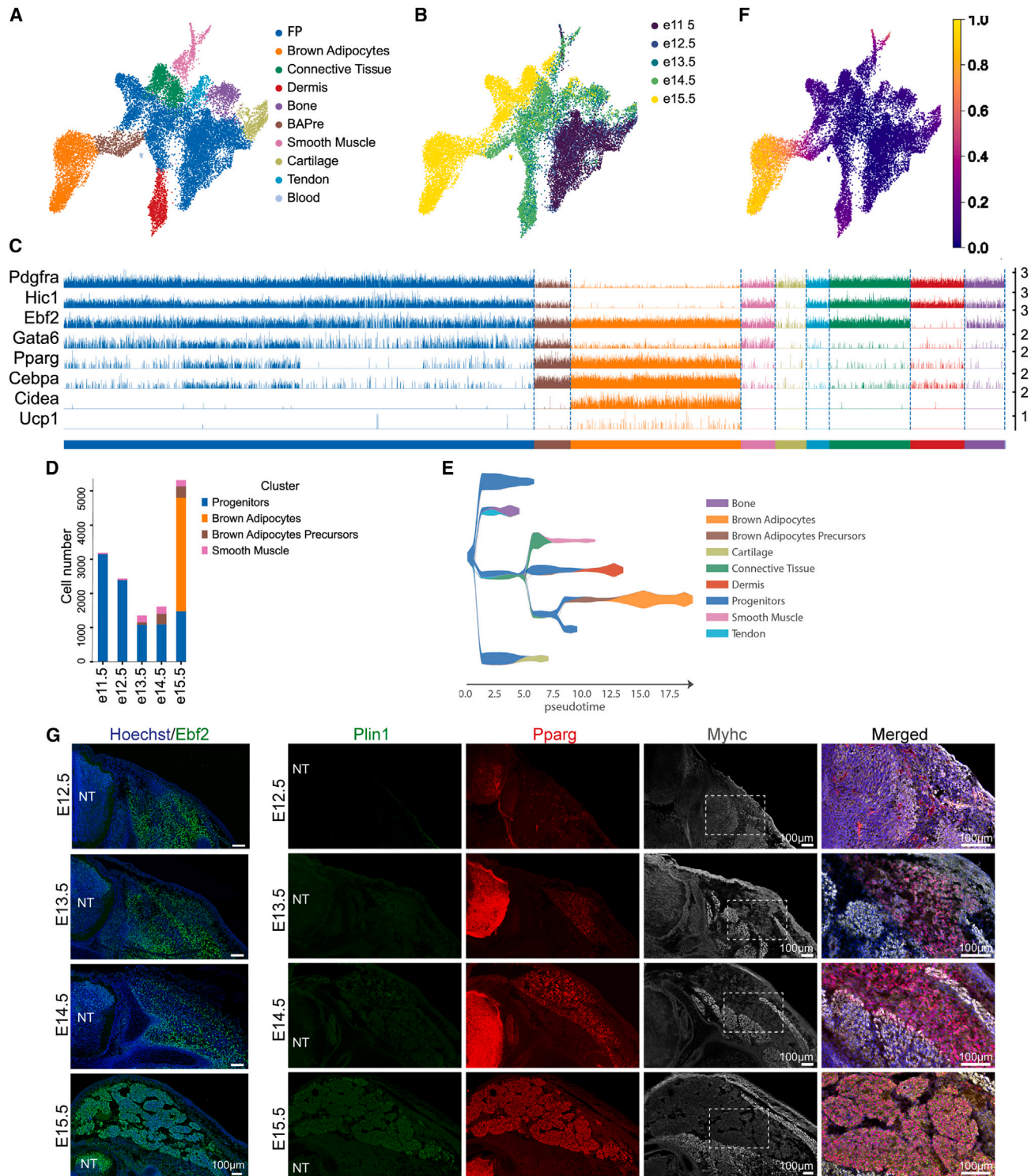
Figure 1. Embryonic development of mouse interscapular BAT

(A and B) UMAP embedding showing cell clusters (A) and embryonic days (B) from dorsal region of mouse embryos. BApre, BA precursors; FPs, fibroblast progenitors.

(C) Tracks plot showing the expression of markers of BA differentiation in clusters shown in (A). Bars show expression level in individual cells.

(D) Barplot showing cell numbers in indicated clusters at 5 time points.

(C) Putative developmental trajectories inferred by the STREAM algorithm.

(legend continued on next page)

Developmental Cell
Resource

 CellPress

BAs from hPSCs by recapitulating developmental cues have also been reported.[19,20] However, to date, a well-characterized roadmap of brown fat lineage development is still missing. Therefore, benchmarking these protocols against the normal trajectory of BA differentiation *in vivo* has not been possible.

In this study, we used single-cell RNA sequencing (scRNA-seq) to profile mouse-somite-derived dorsal tissues (including brown fat, dermis, and skeletal muscle) to investigate brown fat development. We identify a transient stage in BA development characterized by the selective expression of the transcription factor Gata6. We previously developed an efficient protocol recapitulating the development of somitic mesoderm and skeletal muscle progenitors from hPSCs and mouse pluripotent stem cells *in vitro*.[21–23] Building on this protocol and using developmental cues identified in our scRNA-seq data, we now report an efficient strategy to generate GATA6-positive BA precursors (BAPre) and functionally mature BAs *in vitro* from human-induced pluripotent stem cells (hiPSCs).

RESULTS

Single-cell transcriptomic analysis of the dorsal trunk of mouse embryos captures the development of somitic lineages

In mice, interscapular BAT develops in between the dermis, trapezius muscle, pectoralis muscle, and deep dorsal muscle bundles. We isolated dorsal tissues at the forelimb level at E11.5, E12.5, E13.5, E14.5, and E15.5 (Figure S1A) to perform scRNA-seq. For stages E11.5–E14.5, the isolated dorsal tissues include epidermis, dermis, mesenchyme, interscapular brown fat, and skeletal muscle. For the E15.5 time point, to enrich for BAT precursors, we removed the epidermis and underlying dermis before dissociation. Using the inDrops workflow,[24] we generated single-cell transcriptomes from at least 4,000 cells per stage, resulting in a final dataset of 28,244 cells after quality control filtering. Cells from the different time points largely segregate based on transcriptional similarity rather than embryonic age (Figures S1B–D). We identified 17 clusters representing the somitic and non-somitic cell types that reside in the dorsal trunk region of the murine embryo (Figure S1C). Among somite derivatives, we observed clusters of cells that originate from the dermomyotome, including BAs (*Cidea* and *Ucp1*); skeletal muscle (*Myog*, *Ttn*, *Actn2*, and *Myh3*); and dermal fibroblasts (*Twist2*, *Dpt*, and *Crabp1*) (Figures S1E and S1F). In addition, we could annotate clusters of smooth muscle cells (*Cnn1* and *Acta2*); muscle connective tissue (*Ngfr*, *Osr1*, and *Osr2*); cartilage (*Cnmd* and *Col2a1*); endothelial cells (*Cdh5* and *Kdr*); and meninges (*Foxc1*, *Cldn11*, and *Aldh1a2*) (Figures S1E and S1F). Among non-somitic cells, we found macrophages (*Csf1r* and *C1qb*), mast cells (*Srgn* and *Kit*), neutrophils (*Ngp* and *Lccn2*), Schwann cells (*Sox10* and *Mpz*), and epidermal cells (*Krt5* and *Krt14*) (Figures S1E and S1F). In conclusion, our single-cell transcriptomics analysis captured major dermomyotome derivatives including cells of the BA lineage present in the mouse dorsal trunk during embryonic development.

Characterization of the developmental trajectory of BAPre

Most of the somite-derived cells, except endothelial and skeletal muscle cells, lie closely together on the UMAP embedding, suggesting that they have related transcriptional signatures (Figures S1B and S1C). This large group of cells forms a single continuous ensemble including clusters corresponding to cartilage, bone, smooth muscle, connective tissue, dermis, and BAs. All these cell types arise from fibroblastic precursors, thus potentially explaining the similarity of their transcriptomes. We extracted the clusters representing this group of cells and reanalyzed this new dataset in detail. Most of the cells belong to a large central cluster already present at E11.5, which we name Fibroblastic Progenitors (FPs) (Figures 1A and 1B). Cells of this cluster express fibroblast markers including *Pdgfra* or *Hic1* (Figure 1C). Differentially expressed genes of the FP cluster do not contain characteristic lineage markers (Table S1). Moreover, the FP cluster connects to all the different fates, suggesting that it corresponds to a multipotent progenitor population. The FP cluster is linked to a cluster of prospective BAs, which we termed BAPre (Figure 1A). These cells express BAPre markers such as *Ebf2*, *Cebpa*, and *Pparg* (Figures 1C and S2A).[7] The BAPre cluster is connected to a cluster of BAs characterized by the expression of *Cidea* or *Ucp1*, Figures 1C and S2A). The BAPre cluster is first detected at E13.5, and its size progressively increases until E15.5, while the BA cluster is first detected at E15.5 (Figure 1D). Pseudotime analysis supports the existence of a developmental trajectory for the BA lineage that starts from FP cells followed by BAPre and finally BAs (Figure 1F).

We performed an analysis with the STREAM pipeline,[25] which confirmed these putative lineage relationships among clusters (Figure 1E). These conclusions are further supported by an analysis using the Waddington OT pipeline that allows us to characterize the ancestor/descendant sequence based on cell-to-cell transition probabilities and gene expression similarities[26] (Figures S2B and S2C). These analyses support the notion that cartilage, bone, tendon, connective tissue, dermis, and BAs all arise from the FP cluster and that the BA cluster derives from the BAPre cluster (Figures 1E and 1F). Immunofluorescence analysis of E12.5–E15.5 embryos confirmed the expression of Ebf2 not only in the presumptive interscapular brown fat region but also in skeletal muscle and precartilage (Figure 1G).[7] Developing adipocyte precursors expressing Pparg probably corresponding to BAPre start to appear at E13.5 and develop in between the dermis and Myosin heavy chain (MyHC)-expressing muscle fibers (Figure 1G). Perilipin1 (Plin1) staining shows that a small number of preadipocytes start to accumulate lipid vesicles at E14.5. An increasing number of lipid-containing immature adipocytes appears by E15.5 (Figure 1G).

Angueira et al. recently identified progenitors that give rise to BAs in mouse perivascular adipose tissue (pVAT) analyzed by scRNA-seq at E18 and perinatal stages.[27] We reanalyzed their E18 dataset and identified 13 clusters as described in the original study (Figure S2D). We identified a trajectory similar to that

---

(F) UMAP embedding showing diffusion pseudotime.
(G) Immunofluorescence analysis with antibodies against Ebf2, Plin1, Pparg, and MyHC of the developing interscapular BAT in mice. Transverse sections of mouse embryos at the forelimb level. NT, neural tube. n ≥ 3; scale bars, 100 μm.
See also Figures S1 and S2.

observed for the somitic lineages starting with a cluster of FPs (*Pdgfra*), followed by BApre (*Pparg*) and BAs (*Cidea*) (Figures S2E and S2F). *Pi16*, *Cd34*, and *Ly6a*, which were identified as BA progenitor markers in the Angueira report, are also differentially expressed FP cluster in our study (Figure S2G). Using a machine learning classifier trained on the Angueira dataset, we confirmed the similarity between progenitor and BA fates identified in the two studies (Figure S2H). Immunofluorescence analysis at E15.5 confirmed the expression of the adipocyte precursors markers Dpp4, Cd34, and Ly6a at the periphery of the interscapular depot (Figures S2I and S2J). Their location suggested that they might correspond to precursor cells involved in the generation of mature brown fat. Together, these data suggest that the BAs of the interscapular region derive from a multipotent population of FPs expressing markers such as *Pdgfra* that gives rise to an immature population of lineage-restricted precursors (BAPre) appearing around E13.5. Around E15.5, this population starts giving rise to BAs identified by specific markers such as *Cidea*.

Gata6 marks early BAT precursors
To identify specific markers for BAPre, we examined the genes differentially expressed in the BAPre cluster. We noticed that the transcription factor *Gata6*, whose expression in BA development has not been characterized, is found in the top 60 differentially expressed genes. In the BAPre cluster differentially expressed gene list, *Gata6* ranks before *Ebf2*, which has been described as a selective marker for brown adipogenic precursor cells.[7] *Gata6* is restricted to the BA and smooth muscle lineages (Figure 1C). Extraction of the Gata6-expressing cells from the mouse dataset shows that these cells mostly belong to these two lineages, with the majority of them belonging to the FP cluster (Figure 2A). *Gata6*-expressing cells are first detected in the FP and then in the BApre and BA and smooth muscle clusters. *Gata6* expression progressively decreased during the differentiation of BAs (Figure 1C). These observations were confirmed at the protein level by immunofluorescence analysis, which indicated that Gata6 is detected at E12.5 in the presumptive brown fat area under the dermis (Figure 2B). Differentiating Pparg-positive immature adipocytes as well as Pparg-negative adipocyte precursors expressed Gata6 at E14.5 (Figure 2B). At E15.5, most Pparg-positive cells of the forming interscapular BAT had downregulated the Gata6 protein. Strong expression of Gata6 was still observed in Pparg-negative cells at the periphery of BAT, possibly corresponding to BAPre (Figure 2B). Downregulation of both Gata6 mRNA and protein in BAs at E15.5 suggests that Gata6 is transiently expressed during BA differentiation and is downregulated in more mature BAs. We observed a similar expression profile of *Gata6* during BA differentiation in the Angueira dataset (Figure S2F).

To demonstrate that Gata6 is expressed by precursors giving rise to BAs, we used a Gata6-CreERT2:Rosa26-tdTomato mouse line to label Gata6-expressing cells during embryonic development.[28] We induced recombination using tamoxifen injection at E12.5 and analyzed the contribution of labeled cells to BAT at E15.5 (Figure 2C). Immunofluorescence analysis for tdTomato, which labels the descendants of Gata6-expressing cells confirmed that at E12.5, they give rise to heart and lung bud cells as expected (Figure 2C). Among somite-derived cells, tdTomato-positive cells were mostly found in the interscapular

BAT region and not in other somite derivatives such as skeletal muscle, cartilage, or endothelial cells (Figure S3A). No tdTomato-positive cells were detected in skeletal muscle, and we did not observe any overlap with the CD31^{+} population of endothelial cells in BAT (Figures 2C and S3A). tdTomato-positive cells in the interscapular BAT also stained positive for Pparg at E15.5, confirming that these cells are adipocytes (Figure 2C). We also found rare tdTomato-Myh11 double-positive cells next to blood vessels in the interscapular BAT (Figure S3B). This is consistent with the previously reported expression of Gata6 by vascular smooth muscle cells.[29] The number of such potential smooth muscle cells labeled was lower than that expected from the scRNA-seq analysis. These cells could correspond to the recently identified BAPre deriving from the vascular smooth muscle lineage.[30] Also, cells expressing both tdTomato and Dpp4 were observed in the periphery of the forming brown fat mass, supporting the expression of Gata6 by brown fat precursors (Figure S3C). In conclusion, our lineage tracing analysis argues that Gata6-expressing cells present at E12.5 in the mouse dorsal trunk mostly belong to the BA lineage.

To further investigate the origin of these Gata6 precursors, we used a Pax7-Cre:Rosa26-mTmG mouse line to analyze the contribution of Pax7 descendants to Gata6-positive brown fat precursors at E14.5.[31] As expected, dorsal, ventral, and limb skeletal muscle as well as Pparg-expressing prospective BAs precursors were identified as Pax7 descendants (Figure 2D). Membrane GFP also labeled Gata6-positive cells in the brown fat region, indicating that these cells derive from an earlier Pax7-expressing population (Figure 2E). Taken together, our experiments indicate that Pax7-positive somitic progenitors give rise to a Gata6-positive precursor population that differentiates into BAs.

To further examine whether Gata6 expression is conserved in human brown adipogenesis, we performed immunofluorescence analysis on 98- and 135-day-old (estimated post-conceptual age) human fetal tissue from interscapular and scapular regions. We detected the expression of EBF2 and GATA6 in cells adjacent to the skeletal muscle tissue (detected by MyHC antibody) under the dorsal dermis and dispersed between deeper dorsal muscle bundles at 98 days (Figure 3A). As in mice, EBF2 was expressed in a broader territory in the dermis and deeper muscle areas. We also observed a few lipid-filled UCP1- and PPARG-positive adipocytes in the deeper muscle area (Figures 3B and 3C). In these regions, we detected PPARG and GATA6 double-positive cells, supporting the existence of GATA6-positive BA progenitors in humans (Figures 3B and 3C). More mature BAs identified by the presence of lipid droplets, expression of PLIN1, and high expression of PPARG did not express GATA6, suggesting that GATA6 expression is also restricted to an early stage of BA development in humans.

Recapitulation of human BA development *in vitro* from hiPSCs
We next used our scRNAseq data to inform the design of a differentiation protocol, aiming to recapitulate brown adipocyte differentiation from hiPSCs. We previously developed efficient protocols to differentiate human paraxial mesoderm and skeletal muscle from hiPSCs *in vitro*.[21–23] As BAs originate mostly from the paraxial mesoderm and share a common precursor with skeletal muscles in the dermomyotome,[6] we first aimed to
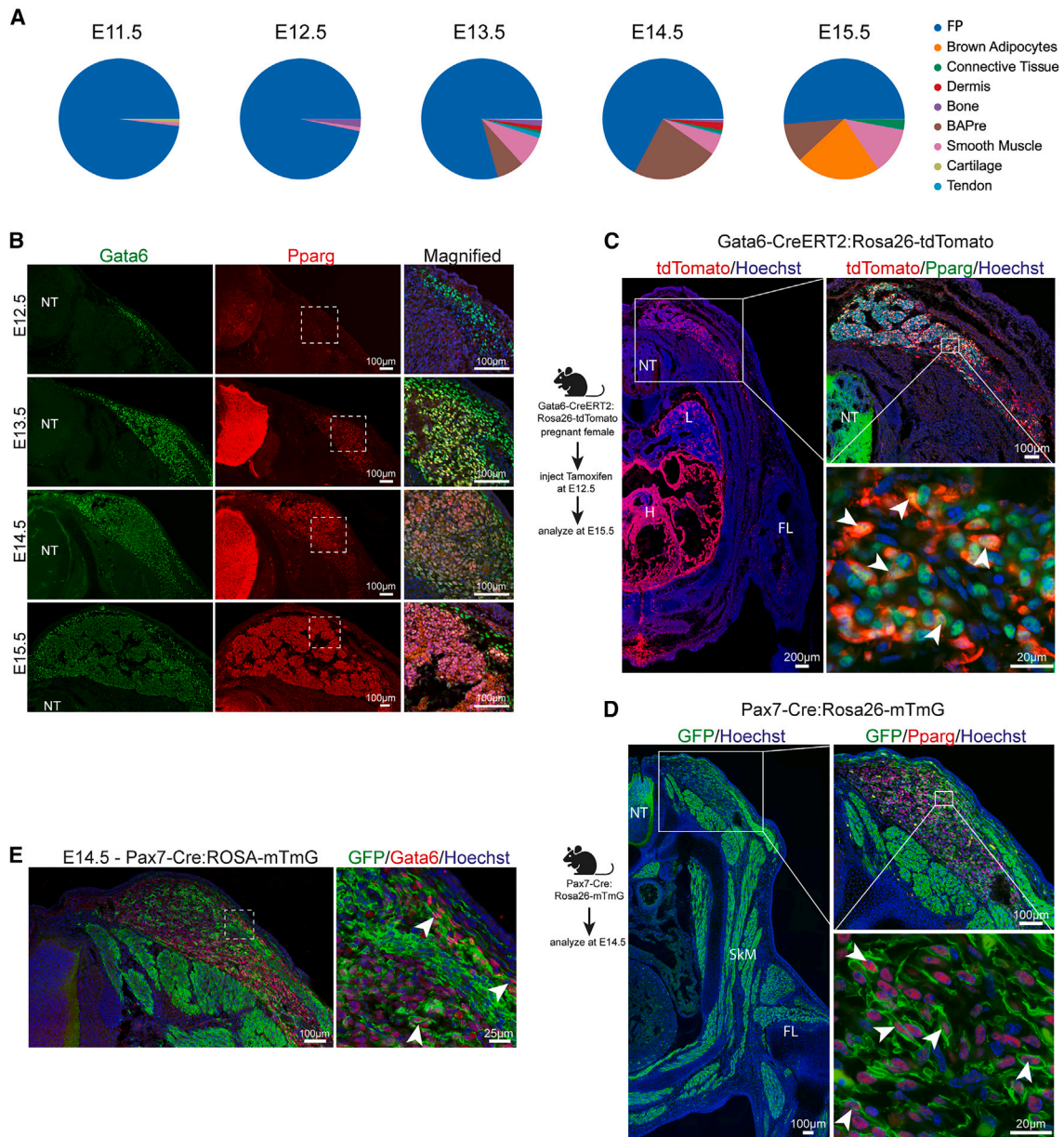
Figure 2. Gata6 is expressed by the developing BA precursors

(A) Proportion of Gata6-positive cells in the clusters.

(B) Immunohistochemical analysis of transverse sections of mouse embryos at the forelimb level with Pparg and Gata6 antibodies. n ≥ 4.

(C) Lineage tracing experiments using Gata6-CreERT2:Rosa26-tdTomato mice. Transverse section at the forelimb level of E15.5 embryos stained with anti-RFP antibody to detect tdTomato-positive cells (left). Magnified image of the transverse section from the interscapular region showing BAT stained with Pparg and RFP (tdTomato) antibody (upper right). Higher magnification image of BAs in the interscapular region showing double-positive cells for Pparg and tdTomato. Arrowheads mark double-positive cells (lower right). n ≥ 3.

(D) Lineage tracing strategy to label Pax7 progeny during mouse development. Transverse section at the forelimb level of E14.5 embryos stained with anti-GFP antibody (left). Transverse section of E14.5 Pax7-Cre:Rosa26-mTmG embryo showing interscapular region stained with antibodies against Pparg and GFP (upper right). Representative high magnification image showing double-positive cells stained for nuclear Pparg and membranous GFP. Arrowheads mark double-positive cells (lower right). n ≥ 3.

(E) Transverse section of E14.5 Pax7-Cre:Rosa26-mTmG embryo showing interscapular region stained with anti-GFP antibody and anti-Gata6. Inset on the right shows magnified view. Arrowheads: double-positive cells. n ≥ 3.

H, heart; L, lung; NT, neural tube; SkM, skeletal muscle.

See also Figures S2 and S3.
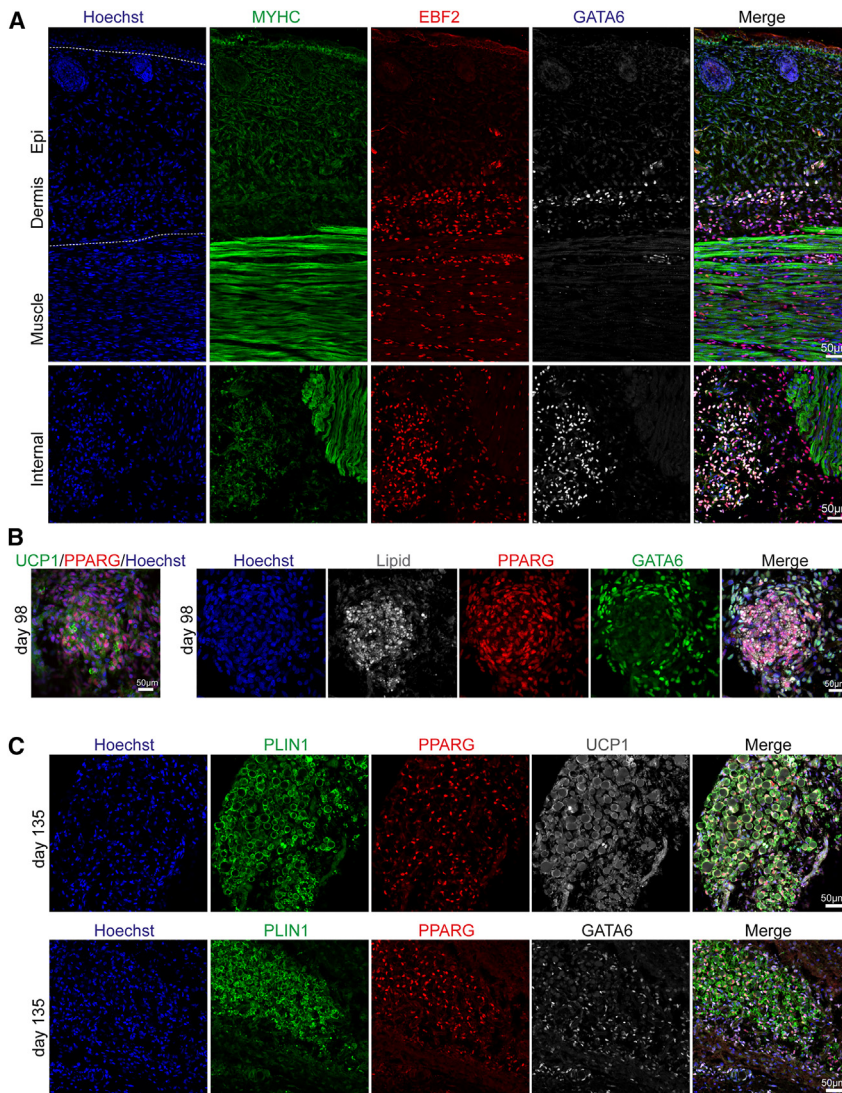
Figure 3. Expression of GATA6 in developing human BAT

(A) Immunofluorescence analysis with anti-MyHC, EBF2, and GATA6 antibodies of human fetal tissues (upper, skin; lower, dorsal muscles) isolated from the scapular region of a 98-day old fetus. $n \geq 3$ sections.

(B) Immunofluorescence analysis of human fetal BAT isolated from the scapular region of a 98-day old fetus stained with anti-UCP1 and PPARG antibodies (left). Consecutive section stained with antibodies against GATA6 in lipid droplets containing adipocytes (right), $n \geq 3$ sections.
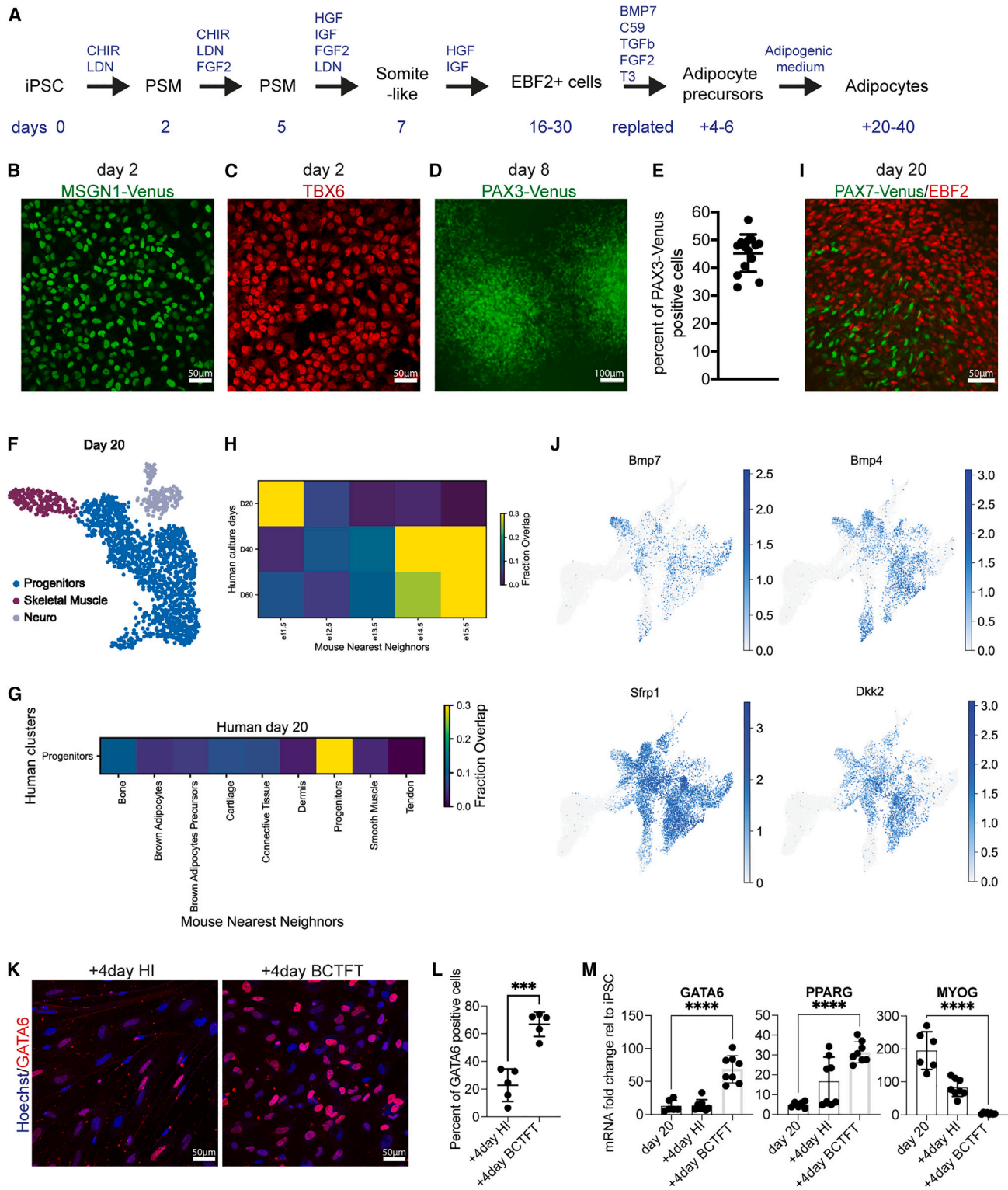
(C) Immunofluorescence analysis of human fetal BAT isolated from the scapular region of a 135-day old fetus. Expression of PLIN1, PPARG, UCP1 (upper), and GATA6 (lower) detected with specific antibodies, $n \geq 3$ sections.

recapitulate the development of Pax-3 positive dermomyotomal cells in vitro. To achieve this, we treated hiPSCs with the Wnt agonist CHIR (CHIR 99021) and the BMP inhibitor LDN (LDN-193189) (Figure 4A). At days 2–3, most of the cells expressed the PSM markers MSGN1 (95% ± 0.4%) and TBX6 (Figures 4B, 4C, and S4A). To further differentiate the PSM cells into dermomyotomal PAX3-positive cells, we treated cultures with insulin growth factor (IGF), fibroblast growth factor (FGF), hepatocyte growth factor (HGF), and LDN.[21,22] To monitor cell differentiation toward the dermomyotome fate, we used CRISPR-Cas9 to knock in a Venus fluorescent reporter into the PAX3 locus (Figure S4B). On day 8, 45% ± 6.7% of the cells started to express Venus (Figures 4D, 4E, and S4C). We further differentiated these cultures in a medium containing HGF and IGF as this treatment promotes the differentiation of somitic PAX7 precursor cells.[21,22] PAX7 appeared around day 14, and at day 20, around 20%–30% of the mononucleated population expressed PAX7 (Figure 4I).[32] To investigate the cell composition of such cultures, we analyzed 1,671 cells from day 20 cultures by scRNA-seq. We observed a major cluster containing cells that

expressed fibroblastic markers such as PDGFRA, HIC1, and EBF2 (Figures 4F and S5D). This cluster also contained a subpopulation of PAX7-positive cells connected to a smaller cluster of differentiating myogenic cells (MYOD1 and MYH3) (Figure S4D). A small cluster of SOX2+ neural cells was also observed at this stage. Using a machine learning classifier trained on the mouse dataset, we observed that the identity of this human progenitor cluster is related to the mouse FP cluster (Figure 4G). Using the classifier trained on mouse dataset, we found that these day 20 iPSC-BA cultures were closely related to mouse E11.5 cells (Figure 4H).[11] BAs and myogenic precursors have undergone lineage commitment by the time Ebf2 protein expression is detected in Myf5-Cre+ lineage cells.[7] Most of the cells of the FP cluster expressing EBF2 are negative for PAX7 at the mRNA and protein levels, and MYF5 is known to be largely co-expressed with PAX7 in our cultures around day 20.[32] This suggests that the adipogenic and myogenic lineages are already separated or in the process of segregating in our 20-day cultures.

We next sought to identify potential signaling pathways involved in brown adipogenesis from the mouse dataset. Mouse knockout experiments have identified BMP activation and Wnt inhibition as important signals required for BA development.[10,33,34] However, these studies have not precisely defined the time window when these cues act on BAPre. We observed the expression of the BMP ligands (Bmp7 and Bmp4) and the Wnt signaling antagonists (Sfrp1, Sfrp2, Sfrp4, and Dkk2) mostly at the FP stage in the mouse dataset (Figures 4J and S5). Expression of these secreted cues was downregulated in more mature cells of the BA lineage. These data suggest that BMP activation and Wnt inhibition are prominently required at the FP stage. Using KEGG pathway analysis, we identified several pathway-specific genes differentially expressed in the FP cluster (Figure S5A). These include genes involved in TGF-β signaling (Tgfbr2 and Gdf10); thyroid hormone

Figure 4. Development of human BA precursors in vitro

(A) Differentiation protocol. + indicates additional days after replating.

(B) Venus signal in MSGN1-Venus hiPSC line on day 2 of differentiation, n = 4.

(C) Immunofluorescence analysis for transcription factor TBX6 on day 2 of differentiation, n = 4.

(D) Venus signal in PAX3-Venus hiPSC line on day 8 of differentiation, n = 7.

(E) FACS analysis quantification of PAX3-Venus positive cells on day 8 of differentiation. Mean ± SD, n = 14.

(legend continued on next page)

signaling (*Creb3l1*, *Gnas*, *Gpx7*, *Creb5*, and *Hsp90b1*); and FGF/PI3K-AKT pathway (*Akt1*, *Igf1*, and *Fgfr1*) (Figures S5A–C). Thus, to recapitulate the sequence of signaling cues to which BAPre are exposed during their differentiation *in vivo*, we dissociated the primary cultures around day 20 of differentiation to eliminate the myofibers and replated the cells in a medium containing BMP7, the Wnt antagonist C-59, TGFb1, FGF2, and triiodothyronine (BCTFT medium) for 4–6 days (Figure 4A). This led to a strong increase in the number of GATA6-expressing cells compared with cells cultured in a medium containing HGF and IGF (Figures 4K and 4L). The cells also showed an upregulation of *GATA6* and *PPARG* and a downregulation of *MYOG* mRNA, suggesting that the BCTFT medium can promote the adipogenic fate while repressing the myogenic fate (Figure 4M).

To follow the differentiation of hiPSCs into BAs, we generated a UCP1-mCherry fluorescent hiPSC reporter line using CRISPR-Cas9. In this knockin line, an mCherry construct was introduced immediately 5′ to the start codon of UCP1 from which it was separated by a P2A peptide. Thus, the reporter is produced from the same transcript as *UCP1* and targeted to the nucleus using an H2B tag (Figure 5A). Using this reporter line, we further differentiated the GATA6-positive progenitors derived in BCTFT medium. We treated the progenitor cultures with an adipogenic cocktail containing 3-isobutyl-1-methylxanthine, ascorbic acid, triiodothyronine, TGFb inhibitor SB431542, dexamethasone, EGF, hydrocortisone, and rosiglitazone for another 20–40 days (Figure 4A).[16] In cultures examined after 40 days in differentiation, large (50–100 μm) UCP1-positive lipid-filled adipocytes started to appear, and the adipocyte number steadily increased over the following 20 days. On day 60 of differentiation, the cultures contained 46% ± 12% of UCP1-mCherry-positive cells (Figures 5B and 5C). Using immunohistochemistry, we showed that 95% of the mCherry-positive cells expressed UCP1 (Figure 5D). PLIN1 and BODIPY staining confirmed that hiPSC-derived BAs (iPSC-BAs) contain multilocular lipid droplets (Figures 5E and 5F). We further confirmed the expressions of BA markers such as *UCP1*, *PPARG*, *CIDEA*, and *PLIN1* after 60 days of differentiation using quantitative real-time PCR in cultures (Figure 5G).

iPSC-BAs contain abundant mitochondria (a characteristic of BAs) as revealed by the immunofluorescence for mitochondrially encoded cytochrome c oxidase II (MT-CO2) and electron microscopy analysis at 60 days of differentiation (Figures 5H and 5I). These cultures contained a fraction of UCP1-negative cells, which expressed EBF2 and/or GATA6 cells, suggesting that these cells might correspond to BAPre cells (Figures 5J and 5K). Periodic acid staining and electron microscopy showed

that at this stage, many cells accumulate glycogen, a characteristic of differentiating BAs (Figures 5L and 5M).[35] Thus, our protocol recapitulates a developmental trajectory similar to that observed for BAT differentiation in mouse embryos, leading to efficient differentiation of hiPSCs into UCP1-expressing BAs in serum-free culture conditions.

scRNA-seq analysis of the human brown adipogenic lineage differentiated *in vitro*

To further characterize the differentiation of hiPSCs into BAs, we performed scRNA-seq of the cultures at days 40 and 60 of differentiation. We analyzed 2,744 and 5,322 cells from 40- and 60-day samples, respectively. At day 40, most of the cells belong to a large cluster that expresses fibroblastic markers such as *PDGFRA* and *HIC1* (Figures S6A and S6B). Using the machine learning classifier trained on the mouse dataset, we confirmed that this cluster, which we term progenitors, is most similar to the mouse FP cluster (Figure S6C). We also detected a cluster of cells expressing BAPre markers (*EBF2*, *CEBPA*, and *PPARG*) most closely related to BAPre and BA clusters according to the classifier. These two clusters express *GATA6*. We also observed a small cluster of skeletal muscle cells (*MYOD1*) and one of the neural cells (*SOX2*). At this stage, *PAX7* expression was undetectable. At day 60, we still observed a large fibroblastic cluster expressing markers such as *PDGFRA* and *HIC1* (Figures 6A and 6B). Comparison to the mouse dataset with the classifier shows that it is closest to the FP cluster (Figure 6C). This cluster is connected to a cluster that expresses *GATA6, EBF2*, and *PPARG* resembling the mouse BAPre cluster. While the classifier analysis shows that this fibroblastic cluster is more similar to the FP cluster, it also shows similarity with the mouse BAPre and BA clusters, suggesting that it corresponds to immature cells of the BA lineage. We also identified a cluster of BAs (*CEBPA*, *CIDEA*, and *UCP1*) most similar to the mouse BA cluster (Figure 6B). Small separate clusters of cartilage (*SOX9*), smooth muscle (*CNN1* and *ACTA2*), and neural cells (*SOX2*) were also observed (Figures S6D and S6E).

We next merged the three time points (days 20, 40, and 60) to generate a UMAP projection and performed a Leiden clustering analysis on this combined dataset (Figures 6C–E). The cell types identified in the clustering analysis of individual time points mostly merged into single clusters defined by cell identity rather than age (compare Figures 6C and S6F). The largest cluster corresponds to the progenitor cluster, which is connected to the clusters of more mature fates. This suggests that the progenitor cluster generated *in vitro* represents multipotent precursors similar to the mouse FP cluster. This cluster is already present

(F) UMAP embedding showing cell clusters in the human *in vitro* cultured cells at day 20.

(G) Results of analysis with a k-NN classifier trained on of mouse embryonic clusters used to predict the identity of the human *in-vitro* cultured progenitors.

(H) Results of analysis with a k-NN classifier trained on clusters of E11.5, E12.5, E13.5, E14.5, and E15.5 mouse embryos used to predict the identity of the human *in-vitro* cultured time points at days 20, 40, and 60.

(I) Immunofluorescence analysis using antibodies against EBF2 and PAX7 on day 20 of differentiation, n = 8.

(J) UMAP embedding showing the expression of a curated list of signaling genes.

(K) Immunofluorescence analysis using an antibody against GATA6 in day 40 cultures in HI medium or adipogenic BCTFT medium for 4 days (+4 represents 4 days after replating). n = 5.

(L) Quantification of GATA6-positive cells in (K). Mean ± SD, n=5, t test, p ≤ 0.001.

(M) Quantitative real-time PCR analysis for *GATA6*, *PPARG*, and *MYOG* on day 20 of differentiation and 4 days after replating in HI medium or adipogenic BCTFT medium (+4 represents 4 days after replating). Mean ± SD, n = 6–8, t test, p ≤ 0.0001.

See also Figure S4 and Table S1.

Developmental Cell
Resource

CellPress
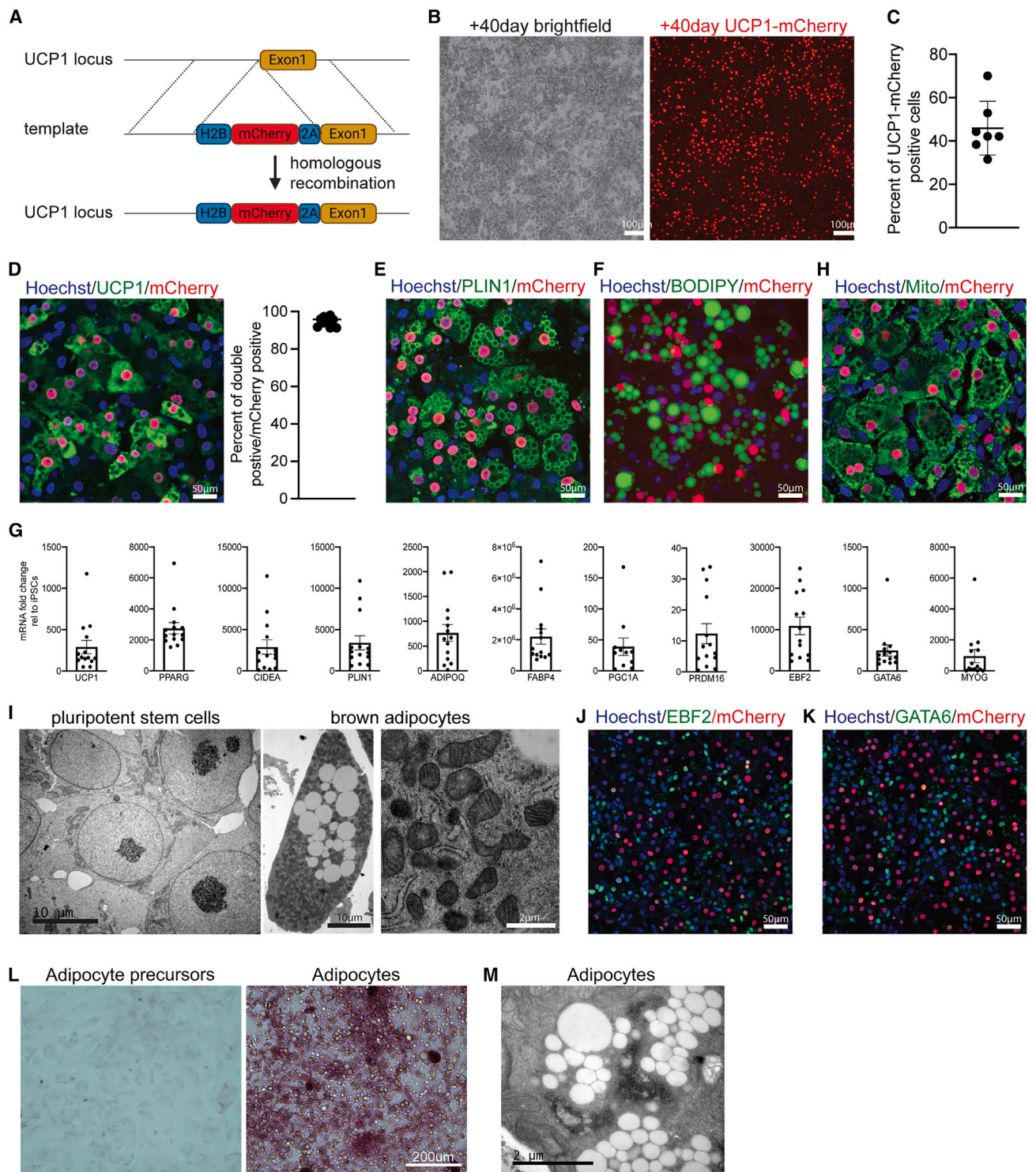
Figure 5. Differentiation of human mature BA _in vitro_

(A) Targeting strategy used to generate UCP1-mCherry hiPSC line.

(B) Brightfield and UCP1-mCherry signal in iPSC-BA cultures on day 60, n ≥ 20.

(C) Quantification of UCP1-mCherry-positive cells in iPSC-BA cultures on day 60. Mean ± SD, n = 7.

(D) Immunofluorescence staining with UCP1 and mCherry antibodies in the UCP1-mCherry knockin iPSC-BA cultures on day 60. Fraction of UCP1 and mCherry double-positive cells from all mCherry-positive cells. n = 10.

(E) Immunofluorescence staining for PLIN1 antibody in the UCP1-mCherry knockin iPSC-BA cultures on day 60. n = 6.

(F) Neutral lipid staining using 0.5 mM BODIPY in iPSC-BA cultures on day 60, n = 3.

(legend continued on next page)

at day 20 and maintained during later stages (Figures 6E and 6F), like the FP cluster of the mouse dataset. Waddington OT analysis of the developmental trajectories of cells differentiating *in vitro* suggests that the progenitor cluster contributes to BAPre and smooth muscle clusters observed at days 40 and 60 as well as to the cartilage identified at day 60 (Figure 6G). It also shows that the day 60 BA cluster likely derives from the BAPre cluster (Figure 6H).

We next directly compared the day 60 iPSC-BA cultures with the mouse scRNA-seq dataset. The list of expressed mouse genes was converted into their human orthologs, and the two datasets were merged and analyzed together using UMAP projection, followed by Leiden clustering. Human and mouse cells identified as FPs, BAPre, and BAs were found in the same clusters in the merged dataset, indicating the similarity of the human cells differentiated *in vitro* to the mouse BA lineage differentiating *in vivo* (Figures S7A–S7C). Clusters of other lineages such as cartilage or smooth muscle also contained both mouse and human cells. Side-by-side comparison of the expression of specific markers of BA differentiation in the same clusters in mouse and human cells shows very similar expression patterns (Figure S7D). Finally, we used the classifier trained on the mouse dataset to compare each time point analyzed *in vitro*, with each of the different mouse embryonic ages analyzed. This suggests that the day 40 cells are closer to mouse cells at E14.5–15.5 and day 60 cells to mouse cells at E15.5 (Figure 4G).

To molecularly characterize the iPSC-BAs that are mostly lost during dissociation in the scRNA-seq analysis, we performed bulk mRNA-seq of undifferentiated hiPSCs and cultures at day 60. In parallel, as a reference for differentiated adipocytes, we performed bulk RNA-seq of human fetal BAT (fBAT) isolated from post-conceptual fetuses aged 115, 122, and 125 days from the interscapular and scapular regions. We used bulk RNA-seq data from iPSC-derived skeletal muscle cultures (iPSC-SkM) as an outgroup.[36] BA-specific genes such as *UCP1*, *CIDEA*, *PARGC1A*, and *DIO2* were specifically expressed in iPSC-BAs and fBAT (Figure 7B). *GATA6* was also detected, suggesting the presence of adipocyte precursors in differentiating cultures (Figure 7A). The top 200 differentially expressed genes in iPSC-BAs corresponded to human WikiPathways related to "PPARG signaling pathway," "Estrogen receptor pathway," and "Thermogenesis" (Figure 7B). When analyzed using the ProFat database,[37] the browning probability of iPSC-BAs was comparable with that of fBAT (Figure 7C). Recently, two studies have described the directed differentiation of BAs from hPSCs.[19,20] Comparison of our iPSC-BAs with the terminally differentiated adipocytes from the two studies—50-day-old adipocytes from Zhang et al. (H9-day 50) and 25-day-old adipocytes from Carobbio et al. (KOLF2-C1-day 25) showed that cells differentiated according to our protocol exhibit a higher degree of similarity to the fBAT and BA gene expression profile (Figures 7D and S7E).

In conclusion, this analysis suggests that a BA lineage developmental trajectory highly similar to that observed for mouse interscapular fat *in vivo* can be recapitulated *in vitro* from human iPSCs.

Functionality of iPSC-BAs

Generally, BAs are characterized by their potential to generate heat in response to a beta-adrenergic stimulus and downstream activation of the cAMP pathway.[38] This activation can be mimicked by treatment with forskolin that activates cAMP signaling.[19,39,40] Day 60 cultures treated with forskolin for 4 hours show increased *UCP1* mRNA levels compared with vehicle-treated cells (Figure 7E). To evaluate the lipolytic activity of the cells, we measured the amount of glycerol released in the medium after forskolin treatment. In comparison to vehicle control-treated cells, forskolin-treated cells showed an increased glycerol release (Figure 7F). To measure the ability of iPSC-BAs to generate heat, we used ERthermAC, a thermosensitive vital fluorescent dye.[39] As temperature increases, the cells display lower ERthermAC fluorescence intensity. We preincubated iPSC-BAs with ERthermAC, treated with PBS or forskolin, and measured the fluorescence intensity of the dye over time. We observed a reduction in dye intensity in forskolin-treated cells compared with vehicle-treated cells (Figure 7G). In contrast, no change in intensity was observed for day 20 BAPre in either condition. Overall, our data demonstrate that iPSC-BAs induce UCP1 expression, undergo lipolysis, and generate heat in response to forskolin activation as normal human BAs.

The process of thermogenesis is driven by the flow of protons through UCP1 in the mitochondrial inner membrane. To examine whether forskolin-induced thermogenesis in iPSC-BAs is coupled to proton leak in mitochondria, we measured oxygen consumption rate (OCR) with a Seahorse metabolic flux analyzer in day 60 cultures (Figure 7H). Upon treatment with oligomycin, an ATP synthase inhibitor, the OCR in cells decreased. When iPSC-BAs were treated with forskolin together with oligomycin, the OCR increased, suggesting that proton leak is increased, leading to higher oxygen consumption (Figure 7H). In contrast, the day 20 precursors showed lower basal respiration levels and did not show increased OCR upon forskolin treatment. As expected, inhibiting the electron transport chain using rotenone (mitochondrial complex I inhibitor) or antimycin (mitochondrial complex III inhibitor) resulted in a drop of OCR (Figure 7H). These analyses support the functionality of human iPSC-BAs differentiated *in vitro*.

DISCUSSION

Studying brown fat lineage development has proven complicated due to the difficulty in identifying intermediate stages in differentiation. In this report, we first characterized the development of interscapular mouse brown fat using scRNA-seq. We

---

(G) Quantitative real-time PCR analysis of iPSC-BA cultures on day 60. Mean ± SD, n = 11–14.

(H) Immunofluorescence staining for mitochondria on iPSC-BA cultures on day 60, n = 5.

(I) Representative transmission electron micrographs of hiPSCs (left) and iPSC-BA (middle and right), n = 3.

(J and K) Immunofluorescence staining with antibodies against EBF2 (J) and GATA6 (K) in UCP1mCherry iPSC-BA cultures on day 60, n = 4.

(L) Periodic acid staining on BA precursors (day 20) and BAs (day 60), n = 3.

(M) Transmission electron microscopy micrographs demonstrating glycogen accumulation in iPSC-BA, n = 3.

See also Figure S5.
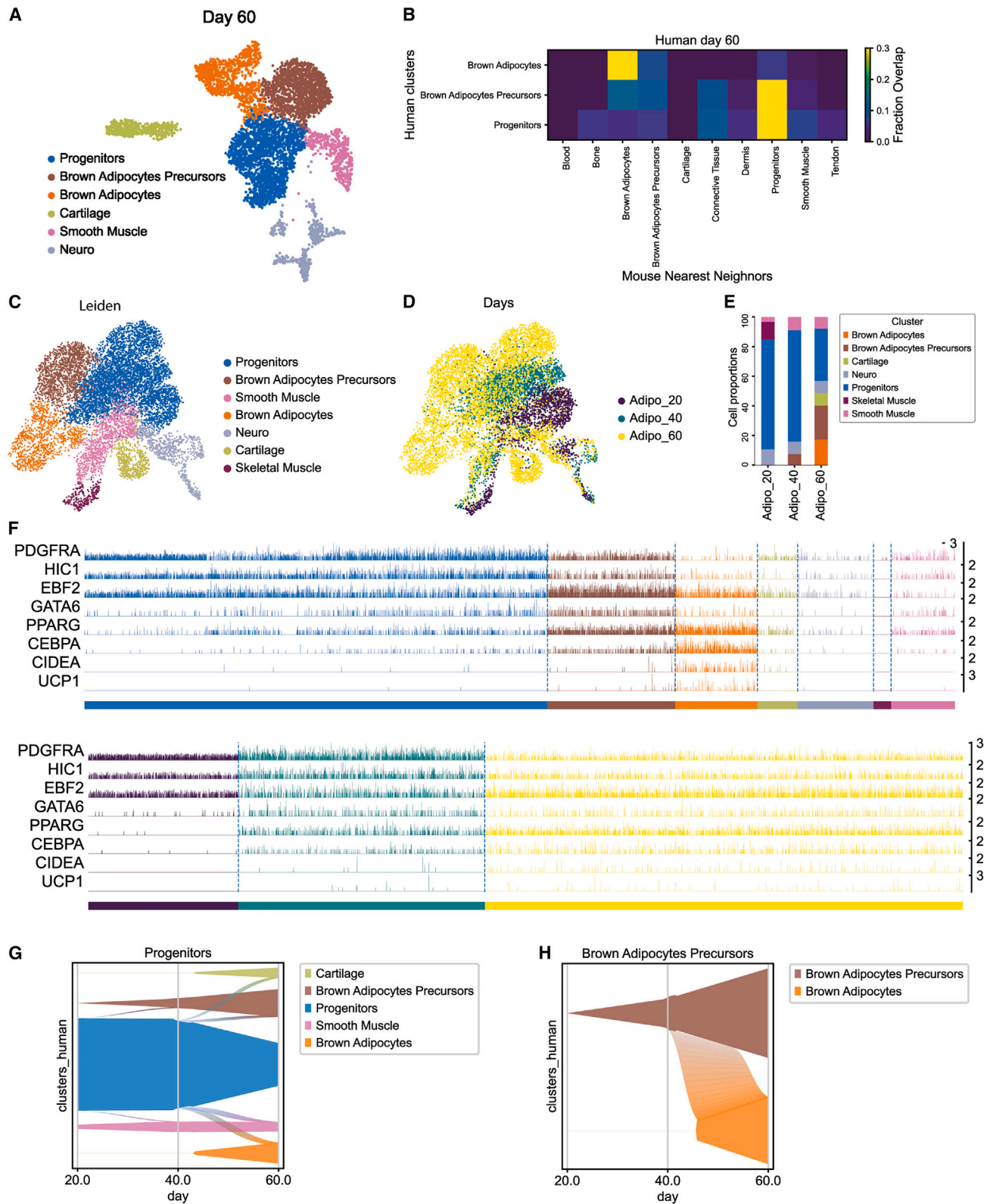
Figure 6. ScRNA-seq analysis of human BAs generated *in vitro*

(A) UMAP embedding showing cell clusters in human *in-vitro* differentiated cells at day 60.

(B) Result of analysis with a k-NN classifier trained on mouse embryo clusters used to predict the identity of human *in-vitro* cultured clusters.

analyzed the development of paraxial mesoderm-derived cell populations in the dorsal trunk that contains interscapular brown fat at the forelimb level of mouse embryos. This analysis identified a previously unrecognized BA differentiation stage characterized by the expression of the transcription factor Gata6. Using bioinformatics tools and lineage tracing analysis in mice, we show that these Gata6+ cells derive from Pax7-precursor cells and generate Pparg-positive preadipocytes that differentiate into Ucp1-positive BAs (Figures 1E and 2B). This scRNA-seq analysis also allowed the identification of specific signaling pathways associated with the Gata6-positive BAs' progenitor state. We used these signaling cues to modify a protocol previously established to differentiate human paraxial mesoderm in vitro.[22] This allowed highly efficient generation of functional human BAs in vitro using defined serum-free culture conditions. ScRNA-seq analysis of the human cells differentiating in vitro shows that they recapitulate a developmental sequence very similar to that observed in mouse in vivo. This sequence results in the production of GATA6-positive BAPre and then to PPARG-positive preadipocytes and finally to UCP1-positive adipocytes that exhibit functional properties characteristic of BAs.

Descriptions of brown fat development were mostly done in mice by lineage tracing, using early Cre drivers such as En1, Pax3, Pax7, myf5, or Pdgfra followed by late analyses identifying brown fat based on morphology or after in vitro culture and qPCR for Ucp1.[6–11,41] These studies showed that brown fat cells mostly derive from Pax3- and Pax7/Myf5-positive progenitors that subsequently downregulate these two genes while expressing Ebf2 and Pdgfra. These analyses identified the origin of BAs in early mouse embryos but provided little information on the developmental trajectory followed by their precursors. Mouse brown fat differentiation has been examined using histochemistry for Pparg, perilipin, or Pdgfra[7] and in situ hybridization with genes such as Cebpa that is selectively expressed by the interscapular depot.[35] These analyses demonstrated that the formation of lipid droplets in brown fat precursors is initiated within glycogen clusters starting around E14.5. This precedes the expression of Ucp1 that occurs around E16.5.[35]

In this report, we perform a direct analysis of the transcriptome of the developing interscapular BA depot in mice. Based on these data, we describe the early stages of BA differentiation trajectory. Our analyses using the STREAM or Waddington OT pipelines[25,26] suggest that BAPre share a common Pdgfra+ precursor with other somite-derived mesenchymal lineages such as dermis, muscle connective tissue, cartilage precursors, and smooth muscle (Figures 1E, S2B, and S2C). This is in line with lineage tracing studies showing that BAs derive from Pdgfra+ cells.[7] In contrast, the skeletal muscle cluster is clearly segregated from the mesenchymal cluster in our dataset. This is

consistent with the early loss of adipogenic potential of the dermomyotomal Pax7-expressing cells that occurs at E11.5 in mice.[11] Our lineage tracing experiments confirm that most of the mouse interscapular brown fat derives from Pax7-expressing precursors[8,11] that can give rise to the Gata6-positive BAPre population. These early Pax7 precursors could correspond to the En1-positive cells of the central dermomyotome previously identified in mice.[10] We reanalyzed a scRNA-seq dataset of developing mouse periaortic BAT and observed a population of Gata6-positive BAPre closely related to the one identified in the interscapular BAT.[27] Interestingly, periaortic BAT receives little contribution from Pax3+ cells and has no contribution from Myf5+ cells.[8] This therefore suggests that different embryonic populations can contribute to the Gata6-positive BAPre.

We identified Gata6 (GATA binding protein 6) as a gene enriched in the BA cluster in mice. Gata6 is a zinc-finger transcription factor that plays an essential role in the development of extraembryonic tissues.[42] Its null mutation in mice leads to lethality shortly after implantation. Gata6 has also been implicated in the development of several organs including heart, lung, gut, pancreas, skeleton, and skin, but its expression during brown fat development has so far not been reported.[28,29,42–45] Gata6 was however identified in silico as a transcription factor potentially regulating the expression of brown-fat-specific genes such as Zic1 and tricarboxylic acid cycle (TCA) cycle enzymes such as citrate synthase (Cs) in the ProFAT database.[37] Also, a GATA recognition motif was identified in ATACseq data of differentiating human adipocytes in vitro.[19] In cardiomyocytes, GATA-6 was shown to associate with PPARA to regulate the expression of the glucose transporter Glut4.[46] Together, these data suggest that Gata6 could play a role in the regulation of energy metabolism in differentiating BAs.

We show that Bmp4/7 and Bmpr1a/2 are enriched in the Gata6-positive progenitors. This is consistent with the well-established role of Bmps in the promotion of brown adipogenesis.[33,47] We also observed transient expression of the Wnt inhibitors Sfrp1,2, and 4 and Dkk2 in the Gata6-positive precursors, consistent with the well-known anti-adipogenic role of Wnt signaling.[34,48] These signals are downregulated as cells differentiate further in the BA lineage. The thyroid hormone and the FGF/IGF1/PI3K pathways that play a role in the control of thermogenesis and BAT development and physiology were also activated in the Gata6 precursors.[49,50] Thus, our data suggest that signaling cues known to be important for brown adipogenesis such as Wnt inhibition and BMP activation act at the Gata6-positive precursor stage.

We previously established an efficient protocol to differentiate hiPSCs to skeletal muscle fate.[21,22] These cells first differentiate to the presomitic (MSGN1) stage,[23] then to the dermomyotome (PAX3) stage, and after 2 weeks in vitro, they start to differentiate

---

(C) UMAP embedding showing the identity of cell clusters in the merged human in-vitro dataset of cultured cells at days 20, 40, and 60.

(D) UMAP embedding showing time points in the merged human in-vitro dataset of cultured cells at days 20, 40, and 60.

(E) Proportions of cell clusters per time points.

(F) Tracks plot showing the expression level of markers genes of the BA lineage in individual cells in the clusters shown in (C) (top) and at the different ages as shown in (D) (bottom).

(G and H) Graphs showing how probability mass flows from the progenitor cluster (G) or from the BAPre cluster (H) to other clusters as a function of time based on Waddington OT transition matrix.

See also Figure S6.

Developmental Cell
Resource

CellPress
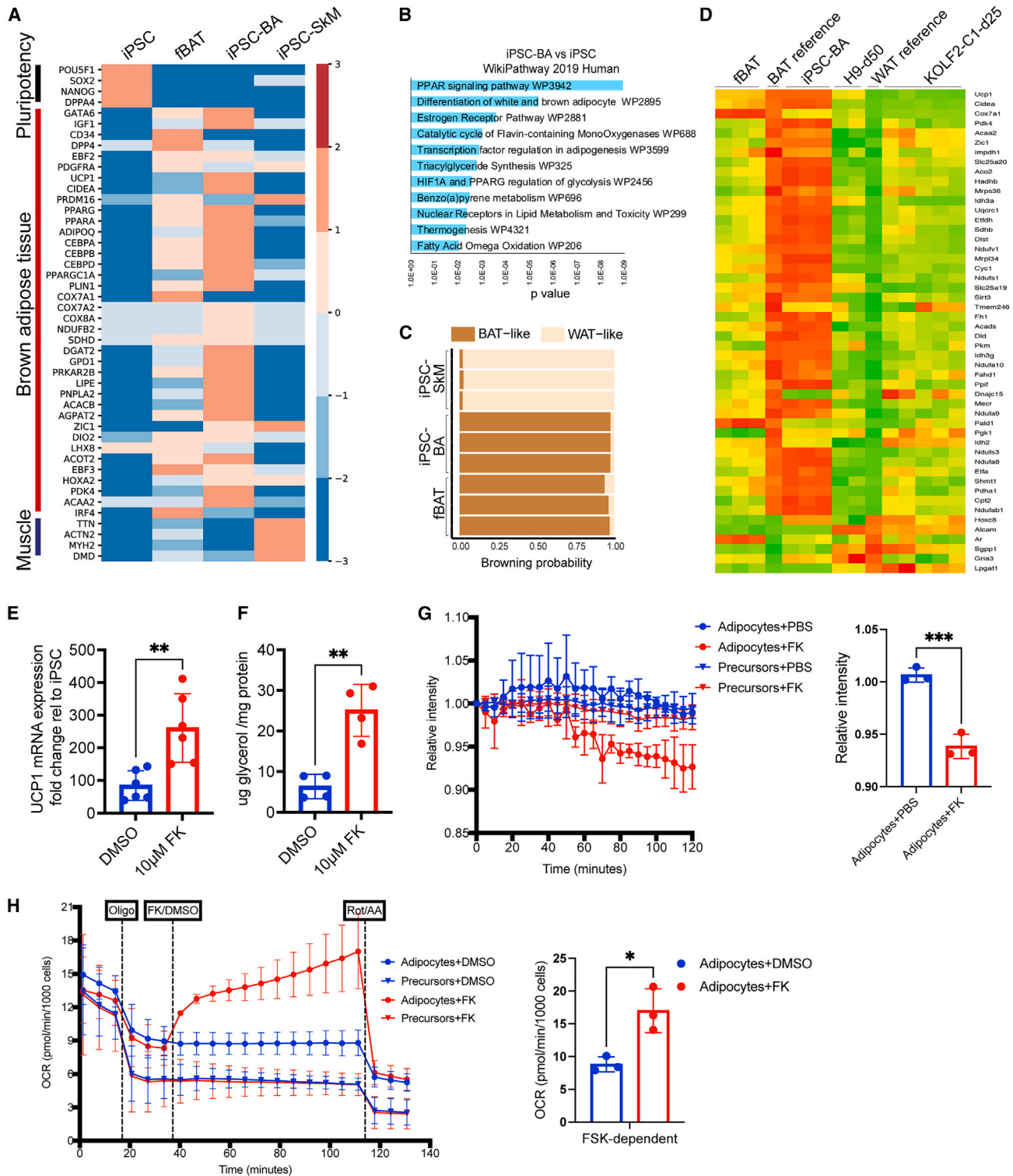
Figure 7. Human BAs generated *in vitro* are functional

(A) Heatmap showing differentially expressed genes. Scale bar represents log normalized read counts.

(B) WikiPathway 2019 Human analysis of top 200 differentially expressed genes (FDR < 0.05, $\log_2|FC| > 6$) in iPSC-BAs compared with iPSCs.

(C) Estimation of browning probability of iPSC-BA, iPSC-SkM, and fBAT using ProFAT database. Numbers represent replicates.

(D) Heatmap comparing transcriptomic profiles of iPSC-BA, fBAT, and hPSC-BAs in Zhang et al.[19] (H9-day 50, 2 replicates) and iPSC-BAs in Carobbio et al.[20] (KOLF2-C1-day 25, 5 replicates).

to PAX7-positive cells. After ~20 days *in vitro*, up to 25% of the culture mononucleated fraction expresses PAX7.[32] Our classifier analyses comparing the mouse embryo dataset with the hiPSCs differentiated *in vitro* suggest that at day 20 of the myogenic differentiation protocol, cells are at a stage equivalent to the E11.5 mouse embryo (Figure 4H) when Pax7-precursors lose their potential to contribute to the adipogenic lineage.[11] Moreover, a majority of day 20 cells appear closely related to the fibroblastic precursors identified in mice (Figure 4G). We therefore decided to treat day 20 cultures, with the signals acting on the fibroblastic population identified in the mouse embryo. Treating replated day 20 cultures for 4–6 days with BMP7, the Wnt antagonist C-59, TGFb1, FGF2, and triiodothyronine (BCTFT medium) leads to a significant increase in *Gata6* expression, while a decrease in *Myog* expression is observed. When these cultures are subsequently exposed to a classical adipogenic medium, they differentiate very efficiently to the BA lineage after 20–40 days. Counting the UCP1-positive cells using fluorescence microscopy in day 60 cultures yields an estimate of ~40%–50% of positive cells. In contrast, we only detected ~1% of cells expressing the *UCP1* transcript in the day 60 scRNA-seq dataset. This is because single-cell dissociation required for scRNA-seq disrupts the mature lipid-filled BAs.[51,52] Nevertheless, our scRNA-seq analysis suggests that in day 60 cultures, ~40% of the sequenced cells belong to the BAPre and BA clusters, while another 40% of the cells are in the progenitor cluster. Together, this suggests that the vast majority (possibly up to 80%–90%) of the day 60 cultures corresponds to cells at various stages of the differentiation of the BA lineage. We also performed bulk RNA-seq of day 60 differentiated cultures in order to include the population of mature BAs that is absent in the scRNA-seq data. Using the ProFAT database,[37] we observed that these cells exhibit a browning probability similar to that of fBAT (Figures 7B and 7E). Finally, these human BAs generated *in vitro* are able to respond to a signal mimicking adrenergic stimulation by increasing Ucp1 expression and glycerol release as well as by increasing temperature and oxygen consumption as their *in vivo* counterparts.[12] This showed that these cells are closely related to fetal and adult human BAs. The comparison of these iPSC-BA cultures with recently generated datasets of mature BAs will require to generate single-nuclei analyses.[51,53]

Comparison of the BAs generated by our protocol with those generated by two other recently published directed differentiation protocols[19,20] suggests that the transcriptional signature of the adipocytes generated in our conditions is closer to endogenous fetal BAs. The choice of agonists and antagonists and their timing of administration described in these papers are not informed by the signaling pattern during BA differentiation as in

our protocol. Zhang et al.[19] used BMP7 and FGF2 in combination with an adipogenic cocktail on day 8 of differentiation to induce BA specification. They also inhibit transforming growth factor β (TGF- β) (our study suggests that the activation of TGF- β signaling promotes adipogenesis at the progenitor stage), and they do not manipulate Wnt signaling. This study claims a differentiation efficiency of 63% of UCP1+ cells based on immunostaining and fluorescence-activated cell sorting (FACS) analysis. However, FACS analysis of lipid-containing BAs is challenging as lipid-containing cells burst open during the dissociation process.[54] In the report by Carobbio et al.,[20] the authors do not inhibit Wnt and do not activate BMP signaling. In this report, the efficiency of adipocyte generation is measured using UCP1 western blotting. However, surprisingly, UCP1 is already detected at day 12 when the human cultures are still extremely immature.

In humans, BAT activity shows an inverse correlation with body mass index and percentage of total body fat.[55,56] Moreover, the graft of ectopic BAT leads to the improvement of glucose metabolism in diabetic or obese mice.[57,58] Our work could therefore help the development of cell therapy strategies involving the graft of human BAs generated *in vitro* for the treatment of obesity, metabolic syndrome, and diabetes.

Limitations of the study

Our scRNA-seq analysis of the iPSC-BA cultures detects few UCP1-positive cells. This is because single-cell dissociation required for scRNA-seq disrupts the mature lipid-filled BAs,[54,55] which are large buoyant cells that cannot be encapsulated using the microfluidics platform used for the inDrops pipeline and are thus poorly respresented in the scRNA-seq dataset. This limitation can be overcome by performing single-nuclei RNA-seq. As an alternative strategy, we estimated the number of UCP1+ cells by quantifying the UCP1-mCherry-positive cells. We propose that Gata6 labels the BA progenitors of the interscapular and perivascular BAT; however, we did not investigate other BAT depots to test whether similar lineage dynamics apply.

STAR★METHODS

Detailed methods are provided in the online version of this paper and include the following:

- KEY RESOURCES TABLE
- RESOURCE AVAILABILITY
  - Lead contact
  - Materials Availability
  - Data and Code Availability

(E) Quantitative real-time PCR analysis for *UCP1* of iPSC-BAs treated with 10 μM forskolin for 4 h. Relative gene expression is shown as relative change to undifferentiated iPSC. Mean ± SD, n = 5, t test, p ≤ 0.01.

(F) Measurement of glycerol release in iPSC-BAs treated with 10 μM forskolin for 4 h. Glycerol amount normalized using total protein amount. Mean ± SD, n = 4, t test, p ≤ 0.01.

(G) Fluorescence intensity of thermosensitive ERthermAC dye in day 20 (precursors) and day 60 (BAs) cultures in response to 10 μM forskolin. Each data point represents mean ± SD, n = 3, t test, p = 0.0009.

(H) Oxygen consumption rate in day 20 (precursors) and day 60 (BAs) cultures in response to 1.5 μM oligomycin, 10 μM forskolin, and 1 μM rotenone and antimycin (Rot/AA). Oxygen consumption rate was normalized by the number of cells per well. Each data point represents mean ± SD, n = 3, t test, p = 0.015.

iPSCs, undifferentiated hiPSCs; fBAT, human BAT from post-conceptual fetuses aged 115, 122, and 125 days ; iPSC-BA, 60-day old iPSC-derived BAs; iPSC-SkM, iPSC-derived skeletal muscle.

See also Figure S7.

Developmental Cell
Resource

CellPress

- ● EXPERIMENTAL MODEL AND STUDY PARTICIPANT DETAILS
  - ○ Human induced pluripotent stem cells
  - ○ Mouse lines
  - ○ Human fetal tissue
- ● METHOD DETAILS
  - ○ Brown adipocyte differentiation
  - ○ Human fetal tissue processing
  - ○ Generation of UCP1-mCherry and PAX3-Venus reporter line
  - ○ RNA extraction, Reverse transcription and real time quantitative PCR
  - ○ Immunocytochemistry
  - ○ Lipid staining
  - ○ Seahorse assay
  - ○ Thermogenesis assay
  - ○ Electron microscopy
  - ○ Glycerol release assay
  - ○ Periodic Acid-Schiff staining
  - ○ Bulk mRNA sequencing
  - ○ Single cell RNA sequencing
- ● QUANTIFICATION AND STATISTICAL ANALYSIS

SUPPLEMENTAL INFORMATION

Supplemental information can be found online at https://doi.org/10.1016/j.devcel.2023.08.001.

AUTHOR CONTRIBUTIONS

J.R. conceptualized the study with O.P. J.R. designed and performed the experiments and analyzed the data. Y.D. analyzed the scRNA-seq data together with J.R. and O.P. J.C. pioneered the *in vitro* differentiation of brown fat in mouse embryonic stem cells. F.M. analyzed the bulk RNA-seq data under the supervision of B.H. C.-H.W. performed the heat generation assay under the supervision of Y.-H.T. Z.A.T. generated the PAX3-Venus hiPSC reporter line. S.G. provided technical support to J.R. for *in vitro* differentiations. A.M.-L. performed the electron microscopy experiments. I.G. provided the human fetal tissues. G.K. and F.M.W. provided the Pax7-Cre:Rosa26-mTmG embryos and GATA6-CreERT2:Rosa26-tdTomato embryos, respectively. J.R. and O.P. wrote the manuscript. O.P. supervised the project.

DECLARATION OF INTERESTS

J.R. and O.P. have filed a patent related to this work.

INCLUSION AND DIVERSITY

We support inclusive, diverse, and equitable conduct of research.

REFERENCES

1. Merklin, R.J. (1974). Growth and distribution of human fetal brown fat. Anat. Rec. *178*, 637–645. https://doi.org/10.1002/ar.1091780311.

2. Heaton, J.M. (1972). The distribution of brown adipose tissue in the human. J. Anat. *112*, 35–39.

3. Lidell, M.E. (2019). Brown adipose tissue in human infants. Handb. Exp. Pharmacol. *251*, 107–123. https://doi.org/10.1007/164_2018_118.

4. van Marken Lichtenbelt, W.D., Vanhommerig, J.W., Smulders, N.M., Drossaerts, J.M., Kemerink, G.J., Bouvy, N.D., Schrauwen, P., and Teule, G.J. (2009). Cold-activated brown adipose tissue in healthy men. N. Engl. J. Med. *360*, 1500–1508. https://doi.org/10.1056/NEJMoa0808718.

5. Virtanen, K.A., Lidell, M.E., Orava, J., Heglind, M., Westergren, R., Niemi, T., Taittonen, M., Laine, J., Savisto, N.J., Enerbäck, S., et al. (2009). Functional brown adipose tissue in healthy adults. N. Engl. J. Med. *360*, 1518–1525. https://doi.org/10.1056/NEJMoa0808949.

6. Seale, P., Bjork, B., Yang, W., Kajimura, S., Chin, S., Kuang, S., Scimè, A., Devarakonda, S., Conroe, H.M., Erdjument-Bromage, H., et al. (2008). PRDM16 controls a brown fat/skeletal muscle switch. Nature *454*, 961–967. https://doi.org/10.1038/nature07182.

7. Wang, W., Kissig, M., Rajakumari, S., Huang, L., Lim, H.W., Won, K.J., and Seale, P. (2014). Ebf2 is a selective marker of brown and beige adipogenic precursor cells. Proc. Natl. Acad. Sci. USA *111*, 14466–14471. https://doi.org/10.1073/pnas.1412685111.

8. Sanchez-Gurmaches, J., and Guertin, D.A. (2014). Adipocytes arise from multiple lineages that are heterogeneously and dynamically distributed. Nat. Commun. *5*, 4099. https://doi.org/10.1038/ncomms5099.

9. Sebo, Z.L., Jeffery, E., Holtrup, B., and Rodeheffer, M.S. (2018). A mesodermal fate map for adipose tissue. Development *145*. https://doi.org/10.1242/dev.166801.

10. Atit, R., Sgaier, S.K., Mohamed, O.A., Taketo, M.M., Dufort, D., Joyner, A.L., Niswander, L., and Conlon, R.A. (2006). Beta-catenin activation is necessary and sufficient to specify the dorsal dermal fate in the mouse. Dev. Biol. *296*, 164–176. https://doi.org/10.1016/j.ydbio.2006.04.449.

11. Lepper, C., and Fan, C.M. (2010). Inducible lineage tracing of Pax7-descendant cells reveals embryonic origin of adult satellite cells. Genesis *48*, 424–436. https://doi.org/10.1002/dvg.20630.

12. Schulz, T.J., and Tseng, Y.H. (2013). Brown adipose tissue: development, metabolism and beyond. Biochem. J. *453*, 167–178. https://doi.org/10.1042/BJ20130457.

13. Samuelson, I., and Vidal-Puig, A. (2020). Studying brown adipose tissue in a human in vitro context. Front. Endocrinol. *11*, 629. https://doi.org/10.3389/fendo.2020.00629.

14. Ahfeldt, T., Schinzel, R.T., Lee, Y.K., Hendrickson, D., Kaplan, A., Lum, D.H., Camahort, R., Xia, F., Shay, J., Rhee, E.P., et al. (2012). Programming human pluripotent stem cells into white and brown adipocytes. Nat. Cell Biol. *14*, 209–219. https://doi.org/10.1038/ncb2411.

15. Takeda, Y., Harada, Y., Yoshikawa, T., and Dai, P. (2017). Direct conversion of human fibroblasts to brown adipocytes by small chemical compounds. Sci. Rep. *7*, 4304. https://doi.org/10.1038/s41598-017-04665-x.

16. Hafner, A.L., Contet, J., Ravaud, C., Yao, X., Villageois, P., Suknuntha, K., Annab, K., Peraldi, P., Binetruy, B., Slukvin, I.I., et al. (2016). Brown-like adipose progenitors derived from human induced pluripotent stem cells: identification of critical pathways governing their adipogenic capacity. Sci. Rep. *6*, 32490. https://doi.org/10.1038/srep32490.

17. Guénantin, A.C., Briand, N., Capel, E., Dumont, F., Morichon, R., Provost, C., Stillitano, F., Jeziorowska, D., Siffroi, J.P., Hajjar, R.J., et al. (2017). Functional human beige adipocytes from induced pluripotent stem cells. Diabetes *66*, 1470–1478. https://doi.org/10.2337/db16-1107.

18. Nishio, M., Yoneshiro, T., Nakahara, M., Suzuki, S., Saeki, K., Hasegawa, M., Kawai, Y., Akutsu, H., Umezawa, A., Yasuda, K., et al. (2012). Production of functional classical brown adipocytes from human pluripotent stem cells using specific hemopoietin cocktail without gene transfer. Cell Metab. *16*, 394–406. https://doi.org/10.1016/j.cmet.2012.08.001.

19. Zhang, L., Avery, J., Yin, A., Singh, A.M., Cliff, T.S., Yin, H., and Dalton, S. (2020). Generation of functional brown adipocytes from human pluripotent stem cells via progression through a paraxial mesoderm state. Cell Stem Cell 27, 784–797.e11. https://doi.org/10.1016/j.stem.2020.07.013.

20. Carobbio, S., Guenantin, A.C., Bahri, M., Rodriguez-Fdez, S., Honig, F., Kamzolas, I., Samuelson, I., Long, K., Awad, S., Lukovic, D., et al. (2021). Unraveling the developmental roadmap toward human brown adipose tissue. Stem Cell Rep. 16, 641–655. https://doi.org/10.1016/j.stemcr.2021.01.013.

21. Chal, J., Oginuma, M., Al Tanoury, Z., Gobert, B., Sumara, O., Hick, A., Bousson, F., Zidouni, Y., Mursch, C., Moncuquet, P., et al. (2015). Differentiation of pluripotent stem cells to muscle fiber to model Duchenne muscular dystrophy. Nat. Biotechnol. 33, 962–969. https://doi.org/10.1038/nbt.3297.

22. Chal, J., Al Tanoury, Z., Hestin, M., Gobert, B., Aivio, S., Hick, A., Cherrier, T., Nesmith, A.P., Parker, K.K., and Pourquié, O. (2016). Generation of human muscle fibers and satellite-like cells from human pluripotent stem cells in vitro. Nat. Protoc. 11, 1833–1850. https://doi.org/10.1038/nprot.2016.110.

23. Diaz-Cuadros, M., Wagner, D.E., Budjan, C., Hubaud, A., Tarazona, O.A., Donelly, S., Michaut, A., Al Tanoury, Z., Yoshioka-Kobayashi, K., Niino, Y., et al. (2020). In vitro characterization of the human segmentation clock. Nature 580, 113–118. https://doi.org/10.1038/s41586-019-1885-9.

24. Klein, A.M., Mazutis, L., Akartuna, I., Tallapragada, N., Veres, A., Li, V., Peshkin, L., Weitz, D.A., and Kirschner, M.W. (2015). Droplet barcoding for single-cell transcriptomics applied to embryonic stem cells. Cell 161, 1187–1201. https://doi.org/10.1016/j.cell.2015.04.044.

25. Chen, H., Albergante, L., Hsu, J.Y., Lareau, C.A., Lo Bosco, G., Guan, J., Zhou, S., Gorban, A.N., Bauer, D.E., Aryee, M.J., et al. (2019). Single-cell trajectories reconstruction, exploration and mapping of omics data with Stream. Nat. Commun. 10, 1903. https://doi.org/10.1038/s41467-019-09670-4.

26. Schiebinger, G., Shu, J., Tabaka, M., Cleary, B., Subramanian, V., Solomon, A., Gould, J., Liu, S., Lin, S., Berube, P., et al. (2019). Optimal-transport analysis of single-cell gene expression identifies developmental trajectories in reprogramming. Cell 176, 928–943.e22. https://doi.org/10.1016/j.cell.2019.01.006.

27. Angueira, A.R., Sakers, A.P., Holman, C.D., Cheng, L., Arbocco, M.N., Shamsi, F., Lynes, M.D., Shrestha, R., Okada, C., Batmanov, K., et al. (2021). Defining the lineage of thermogenic perivascular adipose tissue. Nat. Metab. 3, 469–484. https://doi.org/10.1038/s42255-021-00380-0.

28. Donati, G., Rognoni, E., Hiratsuka, T., Liakath-Ali, K., Hoste, E., Kar, G., Kayikci, M., Russell, R., Kretzschmar, K., Mulder, K.W., et al. (2017). Wounding induces dedifferentiation of epidermal Gata6(+) cells and acquisition of stem cell properties. Nat. Cell Biol. 19, 603–613. https://doi.org/10.1038/ncb3532.

29. Morrisey, E.E., Ip, H.S., Lu, M.M., and Parmacek, M.S. (1996). GATA-6: a zinc finger transcription factor that is expressed in multiple cell lineages derived from lateral mesoderm. Dev. Biol. 177, 309–322. https://doi.org/10.1006/dbio.1996.0165.

30. Shamsi, F., Piper, M., Ho, L.L., Huang, T.L., Gupta, A., Streets, A., Lynes, M.D., and Tseng, Y.H. (2021). Vascular smooth muscle-derived Trpv1(+) progenitors are a source of cold-induced thermogenic adipocytes. Nat. Metab. 3, 485–495. https://doi.org/10.1038/s42255-021-00373-z.

31. Hutcheson, D.A., Zhao, J., Merrell, A., Haldar, M., and Kardon, G. (2009). Embryonic and fetal limb myogenic cells are derived from developmentally distinct progenitors and have different requirements for beta-catenin. Genes Dev. 23, 997–1013. https://doi.org/10.1101/gad.1769009.

32. Al Tanoury, Z., Rao, J., Tassy, O., Gobert, B., Gapon, S., Garnier, J.M., Wagner, E., Hick, A., Hall, A., Gussoni, E., et al. (2020). Differentiation of the human PAX7-positive myogenic precursors/satellite cell lineage in vitro. Development 147. https://doi.org/10.1242/dev.187344.

33. Tseng, Y.H., Kokkotou, E., Schulz, T.J., Huang, T.L., Winnay, J.N., Taniguchi, C.M., Tran, T.T., Suzuki, R., Espinoza, D.O., Yamamoto, Y., et al. (2008). New role of bone morphogenetic protein 7 in brown adipogenesis and energy expenditure. Nature 454, 1000–1004. https://doi.org/10.1038/nature07221.

34. Longo, K.A., Wright, W.S., Kang, S., Gerin, I., Chiang, S.H., Lucas, P.C., Opp, M.R., and MacDougald, O.A. (2004). Wnt10b inhibits development of white and brown adipose tissues. J. Biol. Chem. 279, 35503–35509. https://doi.org/10.1074/jbc.M402937200.

35. Mayeuf-Louchart, A., Lancel, S., Sebti, Y., Pourcet, B., Loyens, A., Delhaye, S., Duhem, C., Beauchamp, J., Ferri, L., Thorel, Q., et al. (2019). Glycogen dynamics drives lipid droplet biogenesis during brown adipocyte differentiation. Cell Rep. 29, 1410–1418.e6. https://doi.org/10.1016/j.celrep.2019.09.073.

36. Al Tanoury, Z., Zimmermann, J., Rao, J., Siero, D., McNamara, H.M., Cherrrier, T., et al. (2021). Prednisolone rescues Duchenne muscular dystrophy phenotypes in human pluripotent stem cells-derived skeletal muscle in vitro. Proc. Natl. Acad. Sci. 118. e2022960118.

37. Cheng, Y., Jiang, L., Keipert, S., Zhang, S., Hauser, A., Graf, E., Strom, T., Tschöp, M., Jastroch, M., and Perocchi, F. (2018). Prediction of adipose browning capacity by systematic integration of transcriptional profiles. Cell Rep. 23, 3112–3125. https://doi.org/10.1016/j.celrep.2018.05.021.

38. Wang, W., and Seale, P. (2016). Control of brown and beige fat development. Nat. Rev. Mol. Cell Biol. 17, 691–702. https://doi.org/10.1038/nrm.2016.96.

39. Wang, C.H., Lundh, M., Fu, A., Kriszt, R., Huang, T.L., Lynes, M.D., Leiria, L.O., Shamsi, F., Darcy, J., Greenwood, B.P., et al. (2020). CRISPR-engineered human brown-like adipocytes prevent diet-induced obesity and ameliorate metabolic syndrome in mice. Sci. Transl. Med. 12. https://doi.org/10.1126/scitranslmed.aaz8664.

40. Kriszt, R., Arai, S., Itoh, H., Lee, M.H., Goralczyk, A.G., Ang, X.M., Cypess, A.M., White, A.P., Shamsi, F., Xue, R., et al. (2017). Optical visualisation of thermogenesis in stimulated single-cell brown adipocytes. Sci. Rep. 7, 1383. https://doi.org/10.1038/s41598-017-00291-9.

41. Sanchez-Gurmaches, J., and Guertin, D.A. (2014). Adipocyte lineages: tracing back the origins of fat. Biochim. Biophys. Acta 1842, 340–351. https://doi.org/10.1016/j.bbadis.2013.05.027.

42. Koutsourakis, M., Langeveld, A., Patient, R., Beddington, R., and Grosveld, F. (1999). The transcription factor GATA6 is essential for early extraembryonic development. Development 126, 723–732.

43. Freyer, L., Schröter, C., Saiz, N., Schrode, N., Nowotschin, S., Martinez-Arias, A., and Hadjantonakis, A.K. (2015). A loss-of-function and H2B-Venus transcriptional reporter allele for Gata6 in mice. BMC Dev. Biol. 15, 38. https://doi.org/10.1186/s12861-015-0086-5.

44. Kozhemyakina, E., Ionescu, A., and Lassar, A.B. (2014). GATA6 is a crucial regulator of Shh in the limb bud. PLoS Genet. 10, e1004072. https://doi.org/10.1371/journal.pgen.1004072.

45. Alexandrovich, A., Qureishi, A., Coudert, A.E., Zhang, L., Grigoriadis, A.E., Shah, A.M., Brewer, A.C., and Pizzey, J.A. (2008). A role for GATA-6 in vertebrate chondrogenesis. Dev. Biol. 314, 457–470. https://doi.org/10.1016/j.ydbio.2007.12.001.

46. Yao, C.X., Xiong, C.J., Wang, W.P., Yang, F., Zhang, S.F., Wang, T.Q., Wang, S.L., Yu, H.L., Wei, Z.R., and Zang, M.X. (2012). Transcription factor GATA-6 recruits PPARalpha to cooperatively activate Glut4 gene expression. J. Mol. Biol. 415, 143–158. https://doi.org/10.1016/j.jmb.2011.11.011.

47. Schulz, T.J., Huang, P., Huang, T.L., Xue, R., McDougall, L.E., Townsend, K.L., Cypess, A.M., Mishina, Y., Gussoni, E., and Tseng, Y.H. (2013). Brown-fat paucity due to impaired BMP signalling induces compensatory browning of white fat. Nature 495, 379–383. https://doi.org/10.1038/nature11943.

48. Bagchi, D.P., and MacDougald, O.A. (2021). Wnt signaling: from mesenchymal cell fate to lipogenesis and other mature adipocyte functions. Diabetes 70, 1419–1430. https://doi.org/10.2337/dbi20-0015.

49. Mullur, R., Liu, Y.Y., and Brent, G.A. (2014). Thyroid hormone regulation of metabolism. Physiol. Rev. 94, 355–382. https://doi.org/10.1152/physrev.00030.2013.

50. Ohta, H., and Itoh, N. (2014). Roles of FGFs as Adipokines in adipose tissue development, remodeling, and metabolism. Front. Endocrinol. 5, 18. https://doi.org/10.3389/fendo.2014.00018.

Developmental Cell
Resource

CellPress

51. Yang Loureiro, Z., Solivan-Rivera, J., and Corvera, S. (2022). Adipocyte heterogeneity underlying adipose tissue functions. Endocrinology *163*. https://doi.org/10.1210/endocr/bqab138.

52. Emont, M.P., Jacobs, C., Essene, A.L., Pant, D., Tenen, D., Colleluori, G., Di Vincenzo, A., Jørgensen, A.M., Dashti, H., Stefek, A., et al. (2022). A single-cell atlas of human and mouse white adipose tissue. Nature *603*, 926–933. https://doi.org/10.1038/s41586-022-04518-2.

53. Sun, W., Dong, H., Balaz, M., Slyper, M., Drokhlyansky, E., Colleluori, G., Giordano, A., Kovanicova, Z., Stefanicka, P., Balazova, L., et al. (2020). snRNA-seq reveals a subpopulation of adipocytes that regulates thermogenesis. Nature *587*, 98–102. https://doi.org/10.1038/s41586-020-2856-x.

54. Aad, G., Abbott, B., Abdallah, J., Abdelalim, A.A., Abdesselam, A., Abdinov, O., Abi, B., Abolins, M., Abramowicz, H., Abreu, H., et al. (2010). Observation of a centrality-dependent dijet asymmetry in lead-lead collisions at sqrt[S(NN)] =2.76 TeV with the ATLAS detector at the LHC. Phys. Rev. Lett. *105*, 252303.

55. Cypess, A.M., Lehman, S., Williams, G., Tal, I., Rodman, D., Goldfine, A.B., Kuo, F.C., Palmer, E.L., Tseng, Y.H., Doria, A., et al. (2009). Identification and importance of brown adipose tissue in adult humans. N. Engl. J. Med. *360*, 1509–1517. https://doi.org/10.1056/NEJMoa0810780.

56. Saito, M., Okamatsu-Ogura, Y., Matsushita, M., Watanabe, K., Yoneshiro, T., Nio-Kobayashi, J., Iwanaga, T., Miyagawa, M., Kameya, T., Nakada, K., et al. (2009). High incidence of metabolically active brown adipose tissue in healthy adult humans: effects of cold exposure and adiposity. Diabetes *58*, 1526–1531. https://doi.org/10.2337/db09-0530.

57. Stanford, K.I., Middelbeek, R.J., Townsend, K.L., An, D., Nygaard, E.B., Hitchcox, K.M., Markan, K.R., Nakano, K., Hirshman, M.F., Tseng, Y.H., et al. (2013). Brown adipose tissue regulates glucose homeostasis and insulin sensitivity. J. Clin. Invest. *123*, 215–223. https://doi.org/10.1172/JCI62308.

58. Gunawardana, S.C., and Piston, D.W. (2012). Reversal of type 1 diabetes in mice by brown adipose tissue transplant. Diabetes *61*, 674–682. https://doi.org/10.2337/db11-0510.

59. Muzumdar, M.D., Tasic, B., Miyamichi, K., Li, L., and Luo, L. (2007). A global double-fluorescent Cre reporter mouse. Genesis *45*, 593–605. https://doi.org/10.1002/dvg.20335.

60. Madisen, L., Zwingman, T.A., Sunkin, S.M., Oh, S.W., Zariwala, H.A., Gu, H., Ng, L.L., Palmiter, R.D., Hawrylycz, M.J., Jones, A.R., et al. (2010). A robust and high-throughput Cre reporting and characterization system for the whole mouse brain. Nat. Neurosci. *13*, 133–140. https://doi.org/10.1038/nn.2467.

61. Dobin, A., Davis, C.A., Schlesinger, F., Drenkow, J., Zaleski, C., Jha, S., Batut, P., Chaisson, M., and Gingeras, T.R. (2013). STAR: ultrafast universal RNA-seq aligner. Bioinformatics *29*, 15–21. https://doi.org/10.1093/bioinformatics/bts635.

62. Liao, Y., Smyth, G.K., and Shi, W. (2014). featureCounts: an efficient general purpose program for assigning sequence reads to genomic features. Bioinformatics *30*, 923–930. https://doi.org/10.1093/bioinformatics/btt656.

63. Love, M.I., Huber, W., and Anders, S. (2014). Moderated estimation of fold change and dispersion for RNA-seq data with DESeq2. Genome Biol. *15*, 550. https://doi.org/10.1186/s13059-014-0550-8.

64. Kuleshov, M.V., Jones, M.R., Rouillard, A.D., Fernandez, N.F., Duan, Q., Wang, Z., Koplev, S., Jenkins, S.L., Jagodnik, K.M., Lachmann, A., et al. (2016). Enrichr: a comprehensive gene set enrichment analysis web server 2016 update. Nucleic Acids Res. *44*, W90–W97. https://doi.org/10.1093/nar/gkw377.

65. Wolock, S.L., Lopez, R., and Klein, A.M. (2019). Scrublet: computational identification of cell doublets in single-cell transcriptomic data. Cell Syst. *8*, 281–291.e9. https://doi.org/10.1016/j.cels.2018.11.005.

66. Tirosh, I., Venteicher, A.S., Hebert, C., Escalante, L.E., Patel, A.P., Yizhak, K., Fisher, J.M., Rodman, C., Mount, C., Filbin, M.G., et al. (2016). Single-cell RNA-seq supports a developmental hierarchy in human oligodendroglioma. Nature *539*, 309–313. https://doi.org/10.1038/nature20123.

67. Polański, K., Young, M.D., Miao, Z., Meyer, K.B., Teichmann, S.A., and Park, J.E. (2020). BBKNN: fast batch alignment of single cell transcriptomes. Bioinformatics *36*, 964–965. https://doi.org/10.1093/bioinformatics/btz625.

68. McInnes, L. (2018). UMAP: uniform manifold approximation and projection for dimension reduction. arXiv. https://doi.org/10.48550/arXiv.1802.03426.

69. Blondel, V.D., Guillaume, J.L., Hendrickx, J.M., de Kerchove, C., and Lambiotte, R. (2008). Local leaders in random networks. Phys. Rev. E Stat. Nonlin. Soft Matter Phys. *77*, 036114. https://doi.org/10.1103/PhysRevE.77.036114.

70. Wolf, F.A., Angerer, P., and Theis, F.J. (2018). SCANPY: large-scale single-cell gene expression data analysis. Genome Biol. *19*, 15. https://doi.org/10.1186/s13059-017-1382-0.

71. Lange, M., Bergen, V., Klein, M., Setty, M., Reuter, B., Bakhti, M., Lickert, H., Ansari, M., Schniering, J., Schiller, H.B., et al. (2022). CellRank for directed single-cell fate mapping. Nat. Methods *19*, 159–170. https://doi.org/10.1038/s41592-021-01346-6.

STAR★METHODS

KEY RESOURCES TABLE

REAGENT or RESOURCE	SOURCE	IDENTIFIER
Antibodies		
Cd34	Thermo Fisher Scientific	14-0341-82;RRID: AB_467210
Dpp4	R&D	AF954-SP;RRID: AB_355739
EBF-2	R&D	AF7006;RRID: AB_10972102
Gata6	RnD	AF1700-SP;RRID: AB_2108901
Gata6	Cell Signaling Technology	5851T;RRID: AB_10705521
GFP	SantaCruz	SC-101536;RRID: AB_1124404
GFP	Abcam	AB13970;RRID: AB_300798
Keratin 14	Biolegend	906001;RRID: AB_2565055
mCherry	OriGene	AB0040-200;RRID: AB_2333093
mCherry	Neuromics	CH22115;RRID: AB_2737138
MTC02	Abcam	AB3298;RRID: AB_303683
Myh11	Alfa Aesar	J64817
MyHCfast	Sigma-Aldrich	M4276;RRID: AB_477190
Perilipin 1	Progen	GP29;RRID: AB_2892611
Perilipin-1	Abcam	AB61682;RRID: AB_944751
PPARG	Thermo Fisher Scientific	MA5-14889; RRID: AB_10985650
RFP	Rockland	600-901-379;RRID: AB_10704808
RFP	Rockland	600-401-379;RRID: AB_2209751
Sca-1/Ly6	R&D	AF1226-SP;RRID: AB_354679
TBX6	Abcam	AB38883;RRID: AB_778274
UCP1	R&D	MAB6158;RRID: AB_10572490
Donkey Anti-Rat IgG H&L (Alexa Fluor® 647) preadsorbed	Abcam	ab150155;RRID: AB_2813835
Donkey anti-Goat IgG (H+L) Secondary Antibody, Alexa Fluor® 488 conjugate	Thermo Fisher Scientific	A-11055;RRID: AB_2534102
Donkey anti-Goat IgG (H+L) Cross-Adsorbed Secondary Antibody, Alexa Fluor 647	Thermo Fisher Scientific	A-21447;RRID: AB_141844
Donkey anti-Sheep IgG (H+L) Cross-Adsorbed Secondary Antibody, Alexa Fluor 594	Thermo Fisher Scientific	A-11016;RRID: AB_2534083
Donkey anti-Sheep IgG (H+L) Secondary Antibody, Alexa Fluor® 488 conjugate	Life Technologies	A-11015;RRID: AB_2534082
Donkey anti-Rabbit IgG (H+L) Highly Cross-Adsorbed Secondary Antibody, Alexa Fluor 488	Thermo Fisher Scientific	A-21206;RRID: AB_2535792
Donkey anti-Rabbit IgG (H+L) Secondary Antibody, Alexa Fluor® 594	Thermo Fisher Scientific	R37119;RRID: AB_2556547
Donkey anti-Rabbit IgG (H+L) Secondary Antibody, Alexa Fluor® 647	Thermo Fisher Scientific	-A-31573;RRID: AB_2536183
Donkey anti-Rabbit IgG (H+L) Highly Cross-Adsorbed Secondary Antibody, Alexa Fluor 555	Thermo Fisher Scientific	A-31572;RRID: AB_162543

Developmental Cell
Resource

⟡ CellPress

Continued

REAGENT or RESOURCE	SOURCE	IDENTIFIER
Alexa Fluor® 488 AffiniPure Donkey Anti-Chicken IgY (IgG) (H+L)	Jackson ImmunoResearch Laboratories	703-545-155;RRID: AB_2340375
Cy™3 AffiniPure Donkey Anti-Chicken IgY (IgG) (H+L)	Jackson ImmunoResearch Laboratories	703-165-155;RRID: AB_2340363
Donkey anti-Mouse IgG (H+L) Highly Cross-Adsorbed Secondary Antibody, Alexa Fluor 647	Thermo Fisher Scientific	A-31571;RRID: AB_162542
Alexa Fluor® 488 AffiniPure Donkey Anti-Guinea Pig IgG (H+L)	Jackson ImmunoResearch Laboratories	706-545-148;RRID: AB_2340472
Bacterial and virus strains		
Promega JM109 Competent E. Coli Cells	Thermo Fisher Scientific	PR-L1001
Biological samples		
Human fetal tissues	University of Washington Birth Defects Research Laboratory (BDRL) under a protocol approved by the University of Washington Institutional Review Board	98 days (H28540), 115 days (H28572), 122 days (H28560), 125 days (H28626)
Chemicals, peptides, and recombinant proteins		
Y-27632 dihydrochloride	R&D Systems	1254/10
CHIR 99021	R&D Systems	4423
LDN-193189	Stemgent	04-0074
FGF-2	PeproTech	450-33
HGF	PeproTech	315-23
IGF-1	PeproTech	250-19
TGFb1	PeproTech	100-21-10
BMP7	Thermo Fisher Scientific	PHC9544
3,3′,5-Triiodo-L-thyronine sodium salt	Sigma-Aldrich	T6397
Porcn Inhibitor II C59	Millipore Sigma	500496
SB431542	Selleck Chemicals	S1067
Dexamethasone	Sigma-Aldrich	D4902
Hydrocortisone	Sigma-Aldrich	H0888
Rosiglitazone	Sigma-Aldrich	R2408
EGF	PeproTech	AF-100-15
3-Isobutyl-1-methylxanthine	Sigma-Aldrich	I7018
ERthermAC	Sigma	SCT057
Oligomycin	Tocris	4110
Forskolin	Sigma-Aldrich	F6886
Antimycin A	Sigma-Aldrich	A8674
Rotenone	Sigma-Aldrich	R8875
4% Paraformaldehyde	Electron Microscopy Sciences	15710
Critical commercial assays		
NucleoSpin® RNA kit	Macherey and Nagel	740955
iScript™ cDNA Synthesis Kit	Bio-Rad	1708891
iTaq™ Universal SYBR® Green Supermix	Bio-Rad	172-5124
Deposited data		
Single cell RNA seq data	This paper	NCBI GEO:GSE185623
Bulk RNA seq data	This paper	NCBI GEO:GSE185518
Single cell analysis code	This study	https://doi.org/10.5281/zenodo.8071624

Continued

REAGENT or RESOURCE	SOURCE	IDENTIFIER
Experimental models: Cell lines		
NCRM-1 (NIH CRM control iPSC line (male)) human iPSC	RUCDR Infinite Biologics	ND50028
NCRM-1-UCP1-H2B-mCherry – 2 clones	This paper	N/A
NCRM-1-PAX3-NLS-Venus – 2 clones	This paper	N/A
Experimental models: Organisms/strains		
Mouse: Pax7-iCre/+;Rosa26-mTmG/+	This study; Gabrielle Kardon Lab	N/A
Mouse: Gata6-EGFPCreERT2;Rosa26-fl/STOP/fl-tdTomato	This study; Fiona Watt Lab	N/A
Mouse: wildtype CD1 IGS mice	Charles River	022
Oligonucleotides		
Quantitative real-time PCR primers	This study	Table S2
Recombinant DNA		
PSpCas9 (BB)-2A-GFP(PX458)	Addgene	48138
pUC19 vector backbone	New England Biolabs	E5510S
pUC19-5'HA-H2B-mCherry-P2A-3'HA	This study	N/A
Software and algorithms		
ImageJ	Image J	https://imagej.nih.gov/ij/
Prism 9	GraphPad	https://www.graphpad.com
kNN-classifier	Diaz-Cuadros et al.[23]	N/A
Stream	Chen et al.[25]	N/A
Waddington-OT kernel	Schiebinger et al.[26]	N/A
ProFAT webtool	Cheng et al.[37]	N/A
FastQC (v0.11.9) and used STAR RNA-seq aligner (v2.7.3a)	Dobin et al.[61]	N/A
featureCounts (v2.0.1)	Liao et al.[62]	N/A
DESeq2 package (v 1.22.2)	Love et al.[63]	N/A
EnrichR	Kuleshov et al.[64]	N/A
Scrublet	Wolock et al.[65]	N/A
Scanpy (v.1.6.0)	Wolf et al.[70]	N/A
Cellrank	Lange et al.[71]	N/A

RESOURCE AVAILABILITY

Lead contact
Further information and requests for resources and reagents should be directed to and will be fulfilled by the lead contact, Olivier Pourquié (pourquie@genetics.med.harvard.edu).

Materials Availability
Plasmids and cell lines generated in this study are available from the lead contact upon request.

Data and Code Availability
- Single-cell RNA-seq data have been deposited at NCBI GEO: GSE185518 and are publicly available. Accession number is also listed in the key resources table.
- Microscopy data reported in this paper will be shared by the lead contact upon request.
- Raw and processed Bulk RNA-seq data have been deposited at NCBI GEO: GSE185623 and are publicly available. Accession number is also listed in the key resources table.
- Single cell RNA sequencing data analysis code has been deposited at Github; https://github.com/PourquieLab/Djeffal_Rao_2023.git and is publicly available. DOIs are listed in the key resources table.
- Any additional information required to reanalyze the data reported in this paper is available from the lead contact upon request.

Developmental Cell
Resource

CellPress

EXPERIMENTAL MODEL AND STUDY PARTICIPANT DETAILS

Human induced pluripotent stem cells

NCRM1 (NIH CRM control iPSC line (male)) human iPSC and other cell lines were routinely cultured on Matrigel (Corning, 354263) coated culture plates (Corning, 353046) in mTeSR (Stemcell Technologies, 85850) at 37°C and normaxia. Upon confluency, cultures were dissociated into single cells using Accutase (Corning, 25-058-C). Cells were seeded on Matrigel coated culture plates in mTeSR supplemented with 10μM Y-27632 dihydrochloride (R&D Systems, 1254/10) at a density of 20,000/cm2 for routine maintenance of iPSC lines. On the following day, medium was replaced with mTeSR only and medium was changed every day. Cultures became confluent every fourth day and were passaged as described above. For freezing, cultures were dissociated into single cells with Accutase and frozen in NutriFreez D10 Cryopreservation Medium (Biological Industries, 01-0020-50).

Mouse lines

Mice were bred and maintained under standard conditions. Pax7-iCre/+;Rosa26-mTmG/+ embryos were generated by crossing Rosa26-mTmG/mTmG[59] males with Pax7-iCre/+ females in timed matings and embryos were collected at E14.5. Gata6-EGFPCreERT2 mice were generated by knocking an EGFPCreERT2 cassette into the endogenous Gata6 locus as reported previously.[28] They were crossed with Rosa26-fl/STOP/fl-tdTomato mice.[60] For lineage tracing experiments, pregnant females were injected intraperitoneally with 50 lg/g of tamoxifen (Sigma) at E12.5 and embryos were collected at E15.5. For experiments other than lineage tracing, wildtype CD1 IGS mice (Charles River) were used.

Human fetal tissue

Human fetal tissues were obtained by the University of Washington Birth Defects Research Laboratory (BDRL) under a protocol approved by the University of Washington Institutional Review Board. BAT tissues were isolated at 98 days (H28540), 115 days (H28572), 122 days (H28560), 125 days (H28626) and 135 days estimated post-conceptual age from the interscapular and scapular region. Informed consent was obtained for use of human tissues in research.

METHOD DETAILS

Brown adipocyte differentiation

iPSCs were differentiated into presomitic mesoderm as described previously[22]. Briefly, confluent maintenance cultures were dissociated into single cells using Accutase (Corning, 25-058-C) and cells were seeded at a density of 30,000-33,000/cm2 on Matrigel (Corning, 354263) coated culture plates (Corning, 353046) in mTeSR (Stemcell Technologies, 85850) supplemented with 10μM Y-27632 dihydrochloride (R&D Systems, 1254/10). Next day, the cells formed small compact colonies. On day 0 of differentiation, to induce presomitic mesoderm, cells were treated with CL medium [DMEM/F12 GlutaMAX (Thermo Fisher Scientific, 10565042) + 1% Insulin-Transferrin-Selenium (Gibco, 41400045) + 3μM CHIR 99021 (R&D Systems, 4423) + 0.5μM LDN-193189 (Stemgent, 04-0074)]. Cells were treated with CL medium for 3 days and medium was refreshed every day. On day 3 of differentiation, cells were changed to CLF medium [CL medium + 20ng/ml FGF-2 (PeproTech, 450-33)]. Cells were treated with CLF medium for 3 days and medium was changed every day.

To further differentiate presomitic mesoderm cells to dermomyotomal fate, cells were changed to HIFL medium [DMEM high glucose (Thermo Fisher Scientific, 11965-118) + Penicillin/Streptomycin (Life Technologies, 15140122) + 15% KnockOut™ Serum Replacement (Life Technologies, 10828-028) + NEAA (Thermo Fisher Scientific, 11140-050) + 0.01mM 2-Mercaptoethanol (Life Technologies, 21985-023) + 10ng/ml HGF (PeproTech, 315-23) + 2ng/ml IGF-1 (PeproTech, 250-19) + 20ng/ml FGF-2 (PeproTech, 450-33) + 0.5μM LDN-193189 (Stemgent, 04-0074)]. Cells were treated with HIFL for two days and medium was changed every day. To let the PAX3 expressing dermomyotomal cells into myogenic and non-myogenic lineages, cells were changed to HI medium (HIFL medium without FGF-2 and LDN-193189) and medium was changed every day.

On day 16-30 of differentiation, cells were replated to differentiate cells into BA lineage. Cultures were dissociated into single cells with 2.5mg/ml Collagenase, (Type IV, Thermo Fisher Scientific, 17104019) and 0.05% Trypsine EDTA (Thermo Fisher Scientific, 25200-056) in PBS (Gibco, 14190) and filtered through a 30 μm (CellTrics, 04-0042-2316) filter and seeded on Matrigel coated plates at a density of 60,000-100,000/cm2 in BCTFT medium [DMEM high glucose (Thermo Fisher Scientific, 11965-118) + Penicillin/Streptomycin (Life Technologies, 15140122) + 5% KnockOut™ Serum Replacement (Life Technologies, 10828-028) + 1% Insulin-Transferrin-Selenium (Gibco, 41400045) + 10 ng/ml FGF-2 (PeproTech, 450-33) + 10ng/ml BMP7 (Thermo Fisher Scientific, PHC9544) + 20nM Porcn Inhibitor II, C59 (Millipore Sigma, 500496) + 10ng/ml TGFb1 (PeproTech, 100-21-10) + 2nM 3,3′,5-Triiodo-L-thyronine sodium salt (Sigma-Aldrich, T6397)]. Cells were treated with BCTFT for 4-6 days and medium was refreshed every day. Adipocyte precursors were either frozen to be used later or differentiated into adipocytes. For freezing, cultures were dissociated into single cells using 0.05% Trypsine EDTA (Thermo Fisher Scientific, 25200-056) in PBS (Gibco, 14190) and cells were frozen in NutriFreez D10 Cryopreservation Medium (Biological Industries, 01-0020-50).

To differentiate adipocyte precursors into adipocytes, cells were cultured in adipogenic medium [DMEM high glucose (Thermo Fisher Scientific, 11965-118) + Penicillin/Streptomycin (Life Technologies, 15140122) + 5% KnockOut™ Serum Replacement (Life Technologies, 10828-028) + 1% Insulin-Transferrin-Selenium (Gibco, 41400045) + 500μM IBMX (3-Isobutyl-1-methylxanthine, Sigma-Aldrich, I7018) + 25.5μg/ml L-Ascorbic acid (Sigma-Aldrich, A4544) + 2nM T3 (3,3′,5-Triiodo-L-thyronine sodium salt,

Sigma-Aldrich, T6397) + 5μM TGFb inhibitor SB431542 (Selleck Chemicals, S1067) + 1μM Dexamethasone (Sigma-Aldrich, D4902) + 10ng/ml EGF (Peprotech, AF-100-15) + 4μg/ml Hydrocortisone (Sigma-Aldrich, H0888) + 1μM Rosiglitazone (Sigma-Aldrich, R2408)] for 30-40 days. Medium was changed every third day.

To perform functional assays and immunofluorescence analysis, 30-40 day old replated cultures were dissociated with 2.5mg/ml Collagenase, (Type IV, Thermo Fisher Scientific, 17104019) and 0.05% Trypsine EDTA (Thermo Fisher Scientific, 25200-056) in 1X Phosphate Buffered Saline (Gibco, 14190) and cells were seeded onto suitable plate format required for the assay.

Human fetal tissue processing
Human fetal tissues were obtained by the University of Washington Birth Defects Research Laboratory (BDRL) under a protocol approved by the University of Washington Institutional Review Board. BAT tissues were isolated at 98 days (H28540), 115 days (H28572), 122 days (H28560), 125 days (H28626) and 135 days estimated post-conceptual age from the interscapular and scapular region. Since adipose depot are relatively small at these stages and are in close contact with adjacent tissues, some surrounding tissue (including connective tissue, skeletal muscle) was also present in the dissected tissue. Tissues were rinsed in 1X Hanks' Balanced Salt Solution (HBSS, Thermo Fisher Scientific, 14185052) before processing. For immunofluorescence analysis, tissues were fixed with 4% Paraformaldehyde (Electron Microscopy Sciences, 15710) overnight at 4°C, washed 3 times in 1X Phosphate Buffered Saline (PBS, Sigma-Aldrich, P5493) and stored at 4°C in PBS supplemented with 0.1% Sodium Azide (Sigma-Aldrich, 71290) until further processing. For bulk mRNA sequencing, tissues were snap frozen in liquid nitrogen and stored at -80°C until further processing.[28,59,60]

Generation of UCP1-mCherry and PAX3-Venus reporter line
UCP1 gene was targeted using the CRISPR-Cas9 system-based genome editing to generate a reporter NCRM1 iPSC line which already had been modified at PAX7 locus to introduce Venus. To target the UCP1 locus, a single guide RNA (sense = CACCG GGTTTGCTGCCCGGCGGAC, antisense = AAACGTCCGCCGGGCAGCAAACCC) targeting the 5' region of the gene was designed using the MIT Crispr Design Tool (www.crispr.mit.edu). The guide RNA was cloned into PSpCas9 (BB)-2A-GFP(PX458) (Addgene, 48138) following protocol from Ran et al., 2013. The final vector was sequence to ensure no mutations were generated during cloning. To generate a targeting vector for homology dependent repair, we cloned 5' and 3' 1kb long homology sequence (HA) flanking a (nuclear localization sequence) NLS region from H2B gene sequence, fluorescent protein mCherry sequence and self-cleaving P2A peptide sequence (5'HA-H2B-mCherry-P2A-3'HA) in a pUC19 vector backbone using Gibson Assembly (New England Biolabs (NEB), E5510S). To mutate the PAM site for the guide RNA, the assembled targeting vector was mutated using site-directed mutagenesis using In-Fusion HD Cloning Plus (Takara, 638909). NCRM1 iPSCs were transfected with both Guide RNA vector (PSpCas9 (BB)-2A-GFP) and targeting vector (pUC19-5'HA-H2B-mCherry-P2A-3'HA) using Lipofectamine™ Stem Transfection Reagent (Thermo Fisher Scientific, STEM00001). 24-hours after transfection, cells were sorted using flow cytometry (S3 cell sorter, Biorad) for GFP positive cells and plated at low density for clonal expansion in Matrigel (Corning, #354263) coated culture plates (Corning, 353046) in mTeSR (Stemcell Technologies, 85850) supplemented with 10μM Y-27632 dihydrochloride (R&D Systems, 1254/10) and Penicillin/Streptomycin (Life Technologies, 15140122). After appearance of small colonies, the colonies were sub-cultured and genotyped using PCR for targeted homozygous insertion of the H2B-mCherry-P2A in the UCP1 locus before the transcription start site. Positive clones were sequenced and clones with no undesired mutation were further validated using immunofluorescence and quantitative real-time PCR. Two positive clones were differentiated into adipocytes and expression of UCP1 in mitochondria and mCherry in the nucleus was confirmed. To generate the human PAX3-Venus iPSC line using the CRISPR/Cas9 technology we followed a similar strategy. We generated a Venus knock-in allele by inserting the Venus sequence in front of the coding sequence of exon 1. Guide RNA (sense = 5'-CCGGCCAGCGTGGTCATCCT GGG-3', antisense = 5'-TGCCCCCAGGATGACCACGC TGG-3') targeting the 5' region of the gene was designed using the MIT Crispr Design Tool (www.crispr.mit.edu). The targeting plasmid (pBSKS-2A-3xNLS) was designed to contain NLS sequence, 1.5 kb of the 5' genomic region of the PAX3 gene, 1 kb of the 3' sequence and 2A sequence. Targeting vector, together with the Cas9 plasmid was electroporated into cells by nucleofection and clones were sub-cultured and genotyped using PCR for targeted homozygous insertion of the NLS-Venus-2A in the PAX3 locus.

RNA extraction, Reverse transcription and real time quantitative PCR
Samples were harvested and RNA was extracted using NucleoSpin® RNA kit (Macherey and Nagel, 740955) following manufacturer's instructions. DNA digestion was performed on column and RNA quality and concentration was measured using Nanodrop. For reverse transcription, 1ug RNA was in a 20ul reaction volume to generate cDNA using iScript™ cDNA Synthesis Kit (Bio-Rad, 1708891). Typically, cDNA was diluted 1:10 with nuclease free water. For real time quantitative PCR, 3.5ul of cDNA, 1.5ul of 10μM forward and reverse primer mix (300μM of forward and reverse primers) and 5ul of iTaq™ Universal SYBR® Green Supermix (Bio-Rad, 172-5124) was used for 10ul reaction volume. For each sample and gene primer set, 3 technical replicates were performed. PCR primers were designed using primer 3, typically spanning splice junctions wherever possible. Primers were validated for amplification efficiency and specificity using a standard curve and melting curves, respectively. PCRs were run on a Bio-Rad CFX384 thermocycler with the following cycling program: initial denaturation step (95°C for 1 minute), 40 cycles of amplification and SYBR green signal detection (denaturation at 95°C for 5 seconds, annealing/extension and plate read at 60°C for 40 seconds), followed by final rounds of gradient annealing from 65°C to 95°C to generate dissociation curves. Relative gene expression was calculated using ΔΔCt method and RPL37A (ribosomal protein L37a) was used as a housekeeping gene. A list of qPCR primers is provided in Table S2.

Developmental Cell
Resource

CellPress

Immunocytochemistry
Cultured cells
Cells were cultured on Matrigel coated plastic culture plates (Corning, #353046), glass bottom 24-well plates (Cellvis, P24-1.5H-N), μ-Dish 35 mm (Ibidi, 81156) or μ-Plate 24 Well Black (Ibidi, 82406). Cultures were washed with 1X Phosphate Buffered Saline (PBS, Sigma-Aldrich, P5493) and fixed with 4% Paraformaldehyde (Electron Microscopy Sciences, 15710) for 20 minutes at room temperature. Cultures were washed with PBS and stored in PBS supplemented with 0.2% Sodium Azide (Sigma-Aldrich, 71290) until used for immunostaining.

Mouse tissues
Mouse embryos were dissected out at different stages in Hanks' Balanced Salt Solution (HBSS) (Gibco, 14185-052). After several washes in HBBS, embryos were fixed in 4% Paraformaldehyde (Electron Microscopy Sciences, 15710) overnight at 4°C. Embryos were then washed in PBS and transferred to 15% sucrose solution (Sigma-Aldrich, 84097) in PBS overnight at 4°C followed by incubation in 30% sucrose solution for overnight at 4°C. Embryos were then embedded in Tissue-Tek O.C.T. Compound (VWR, 25608-930) and stored at -80°C until sectioned. 10-20μm thick sections were cut and stored at -20°C until used for immunostaining.

Fixed cells or sections were permeabilized using 1% Triton-X (Millipore Sigma, T8787) for 10 minutes at room temperature. Samples were washed in PBS and were incubated in blocking solution [PBS supplemented with 3% donkey serum (Jackson ImmunoResearch, 017-000-121) and 0.1% Triton-X] for 1 hour at room temperature. Samples were then incubated with primary antibody diluted in blocking solution at 4°C overnight. Next day, samples were washed 3 times with PBS for 5 minutes. Samples were then incubated with secondary antibody and Hoechst 33342 (ThermoFisher Scientific, H3570) diluted in blocking solution for 1 hour at room temperature followed by 3 washes with PBS for 5 minutes each. Cultured cell samples were stored in PBS until imaged. Mouse tissue slides were mounted using Fluoromount aqueous mounting medium (Sigma-Aldrich, F4680) and were stored at 4°C until analyzed. Samples were imaged using EVOS FL imaging system (Thermo Fisher Scientific) or LSM780 confocal microscope (Zeiss). A list of primary and secondary antibodies is provided in the key resources table.

Lipid staining
iPSC-BA cultures were washed with 1X Phosphate Buffered Saline (PBS, Sigma-Aldrich, P5493) and fixed with 4% Paraformaldehyde (Electron Microscopy Sciences, 15710) for 20 minutes at room temperature. Cell were then incubated with 0.5mM BODIPY™ (Invitrogen™, D3922) in PBS for 20 minutes at room temperature. Cells were washed 3 times with PBS and visualized with EVOS FL imaging system (Thermo Fisher Scientific).

Seahorse assay
Agilent Seahorse XFe96 Analyzer was used to measure oxygen consumption in live iPSC-BAs and precursor cells following manufacturer's instructions. 30,000 iPSC-BAs and precursor cells were cultured on Matrigel (Corning, 354263) coated Seahorse XF96 cell culture microplates (Agilent Technologies, 101085-004). Assay medium was prepared using Seahorse XF DMEM (Agilent Technologies, 103575-100) supplemented with 1 mM pyruvate (Agilent Technologies, 103578-100), 2 mM glutamine (Agilent Technologies, 103579-100), and 10 mM glucose (Agilent Technologies, 103577-100). Basal respiration was measured 3 times in the assay medium. Cells were then treated with 1.5μM Oligomycin (Tocris, 4110) and 3 measurements were taken. Cells were then treated with 10μM Forskolin (Sigma-Aldrich, F6886) or DMSO (Sigma-Aldrich, D2650) and oxygen consumption rate (OCR) was measured for 70 minutes (12 measurements). To block the electron transport chain, cells were then treated with 1μM Rotenone (Sigma-Aldrich, R8875) and Antimycin A (Sigma-Aldrich, A8674) for 3 measurements. Cells were then washed with 1X Phosphate Buffered Saline (PBS, Sigma-Aldrich, P5493) and fixed with 4% Paraformaldehyde (Electron Microscopy Sciences, 15710) for 10 minutes at room temperature. Seahorse XF96 cell culture microplates were imaged for DAPI and mCherry using GE INCELL Analyzer 2200 Widefield High-Content Imager. Cells were automatically segmented using custom code in Fiji and number of DAPI and mCherry positive cells were quantified. OCR data from each well was normalized with DAPI positive cell number in each well. Four replicates were performed. Each experiment consisted of 40 technical replicates for each cell type.

Thermogenesis assay
iPSC-BAs and iPSC precursors were cultured on Matrigel (Corning, 354263) coated 96-well Black Clear-Bottom Plates (Corning, 3603) and were incubated in DMEM/H with 250 nM ERthermAC (Sigma, SCT057) for 30 min at 37°C. After washing with PBS, fresh 90μl DMEM/H without phenol red was added prior to imaging. Fluorescence in stained cells were detected with a GloMax Discover Multimode Detection System (Promega) using 520 nm excitation and emission at 590 nm. Temperature inside the machine was equilibrated at 25°C. After measuring 3 points of basal fluorescence, 10μl forskolin (final concentration 10μM, F6886, Sigma) was added to initiate thermogenesis.10 μl PBS was added for vehicle control group. Fluorescence was recorded every 5 min over 120 min. Results are interpreted as relative intensity (intensity was normalized to basal measurements).

Electron microscopy
iPSC-BAs were rinsed with 0.1M Phosphate buffer pH 7.5 and fixed in 2.5% glutaraldehyde (Sigma, G7651) in 0.1M phosphate buffer at 4°C, for 2 days. Samples were washed in 0.1M phosphate buffer and post-fixed in 1% osmic acid in 0.1M phosphate buffer for 1 hour at room temperature. Dehydration was performed by serial incubation in 50%, 70%, 80%, 95% and 100% ethanol before incubation in propylene oxide for 30 minutes. Samples were impregnated by incubation in propylene oxide/araldite (1:1 v/v) for

60-90 min, in propylene oxide/araldite (1:2 v/v) for 1 hour and in 100% araldite overnight at 4°C. The samples were finally incubated in Araldite which was allowed to polymerize for 24 hours at 56°C. Ultrathin sections (85nm) were cut with a ultracut Leica EM UC. Sections were contrasted 8 min with 2% uranyl acetate and 8 min with lead citrate (Reynolds). All pictures were taken with the Zeiss EM 900 microscope and a GATAN camera (Orius SC 1000).

Glycerol release assay

iPSC-BAs were cultured in a (Corning, 354263) coated 96-well culture plate (Genesee Scientific, 25-109). Cells were serum starved for 16 hours and cultured in serum-free DMEM/F12 GlutaMAX (Thermo Fisher Scientific, 10565042) containing 0.5% BSA. Next day, cells were washed with KRB-HEPES buffer [118.5 mM NaCl, 4.75 mM KCl, 1.92 mM $CaCl_2$, 1.19 mM $KH2PO_4$, 1.19 mM $MgSO_4$, 25 mM $NaHCO_3$, 6 mM glucose and 10 mM HEPES, pH 7.4] containing 4% fatty-acid-free BSA (Bioworld, 22070017-1). Cells were treated with DMSO or 10µM Forskolin in KRB-HEPES buffer supplemented with 4% fatty-acid-free BSA for at 37°C, 5% CO_2 for 4 hours. Cell culture medium was collected for glycerol measurement using the free glycerol reagent (Sigma-Aldrich, F6428) following manufacturer's instructions. A standard curve was generated using Glycerol Standard Solution (Sigma-Aldrich, G7793). Test samples, standards and water control were incubated with the Free Glycerol Reagent for 5 minutes at 37°C and absorbance was recorded at A540 using a spectrophotometer. To normalize with total protein content, Bradford assay was performed using DC Protein Assay (Biorad, 500-0116) following manufacturers protocol.

Periodic Acid-Schiff staining

To stain glycogen in differentiating iPSC-BAs, cells were treated with Periodic Acid-Schiff stain (Sigma, 395B). iPSC-BAs were fixed with 4% paraformaldehyde (Electron Microscopy Sciences, 15710) at room temperature for 15 minutes. Fixed cells were washed several times with distilled water and immersed in Periodic Acid Solution for 5 minutes at room temperature. Cells were then washed in distilled water and incubated with Schiff's Reagent for 15 minutes at room temperature. Cells were washed in running tap water for 5 minutes. Stained cells were visualized in brightfield using EVOS FL imaging system (Thermo Fisher Scientific).

Bulk mRNA sequencing

UCP1-mCherry knock-in line was differentiated into BAs as described above. Cells were harvested on day 60 of differentiation and RNA was extracted using NucleoSpin® RNA kit (Macherey and Nagel, 740955) following manufacturer's instructions. DNA digestion was performed on column and RNA quality and concentration was measured using Nanodrop. Human fetal tissues were harvested as described above and RNA was extracted using NucleoSpin® RNA kit following manufacturer's instructions.

RNA library preparations and sequencing reactions were conducted at GENEWIZ, LLC. (South Plainfield, NJ, USA). RNA samples received were quantified using Qubit 2.0 Fluorometer (Life Technologies, Carlsbad, CA, USA) and RNA integrity was checked using Agilent TapeStation 4200 (Agilent Technologies, Palo Alto, CA, USA). RNA sequencing libraries were prepared using the NEBNext Ultra II RNA Library Prep Kit for Illumina using manufacturer's instructions (NEB, Ipswich, MA, USA). Briefly, mRNAs were initially enriched with Oligod(T) beads. Enriched mRNAs were fragmented for 15 minutes at 94°C. First strand and second strand cDNA were subsequently synthesized. cDNA fragments were end repaired and adenylated at 3'ends, and universal adapters were ligated to cDNA fragments, followed by index addition and library enrichment by PCR with limited cycles. The sequencing library was validated on the Agilent TapeStation (Agilent Technologies, Palo Alto, CA, USA), and quantified by using Qubit 2.0 Fluorometer (Invitrogen, Carlsbad, CA) as well as by quantitative PCR (KAPA Biosystems, Wilmington, MA, USA).

The sequencing libraries were clustered on a single lane of a flowcell. After clustering, the flowcell was loaded on the Illumina HiSeq instrument (4000 or equivalent) according to manufacturer's instructions. The samples were sequenced using a 2x150bp Paired End (PE) configuration. Image analysis and base calling were conducted by the HiSeq Control Software (HCS). Raw sequence data (.bcl files) generated from Illumina HiSeq was converted into fastq files and de-multiplexed using Illumina's bcl2fastq 2.17 software. One mismatch was allowed for index sequence identification.

For bulk RNA-seq data analysis, we performed quality control on the sequence data (FastQ files) using FastQC (v0.11.9) and used STAR RNA-seq aligner (v2.7.3a)[61] to map the sequenced reads to the human reference genome (GRCh38 release 101 from ENSEMBL). Mapped reads were quantified using featureCounts (v2.0.1).[62] Starting from the raw gene counts, normalization and differential expression analysis were done in the R environment (v3.6.0), using the DESeq2 package (v 1.22.2).[63] Genes were defined as differentially expressed when the false discovery rate was lower than 0.05. Gene Ontology (GO) enrichment analysis was performed on the differentially expressed genes using EnrichR,[64] choosing the WikiPathway 2019 Human resource.

To quantify the thermogenic potential of each sample we relied on the ProFAT webtool.[37] Starting from the raw count matrix, barplot and heatmap, representing the adipose browning capacity of each sample, were generated as standard output of ProFAT.

To produce the heat-map for genes of interest (linked to muscle, pluripotency and BAT) we used normalized read counts produced by DESeq2. To calculate up- or down-regulation, we computed the log difference of the average of the biological replicates against the baseline value (average over all conditions) for each gene. All data generated in this study are available at GSE185518.

Single cell RNA sequencing
Preparation of single cell suspension

Single cell analysis of differentiating iPSCs and mouse embryos cells was performed using inDrops as previously reported (Klein et al.).

Developmental Cell
Resource

CellPress

UCP1-mCherry iPSC line was differentiated into BAs as described above. Cultures were harvested on d20, d40 and d60.

The cultures were washed with PBS (Gibco, 14190) and dissociated into single cells using 2.5mg/ml Collagenase, (Type IV, Thermo Fisher Scientific, 17104019) and 0.05% Trypsine EDTA (Thermo Fisher Scientific, 25200-056) in PBS for 5-15 minutes at 37°C. Dissociated cells were run through 70μm cell strainer (Celltreat, 229483) followed by 30μm cell strainer (CellTrics, 04-0042-2316), spun at 300g for 5 minutes and resuspended in DMEM (Thermo Fisher Scientific, 11965-118) + 5% fetal bovine serum (VWR, 89510-186). Cells were again spun at 300g for 5 minutes and resuspended in DMEM + 5% fetal bovine serum, this was repeated 2-3 times to remove debris. Final resuspension was made in PBS + 0.1% bovine serum albumin (Gibco, 15260-037). Cell density was adjusted to 200,000 cells/ml. For day 20, 2500 cells were collected from each sample. For samples at d40 and d60, at least 3000 cells were collected from each sample from two independent differentiations.

For analyzing mouse embryonic tissues, embryos were collected on embryonic day (E) 11.5, 12.5, 13.5, 14.5 and 15.5 from wild-type CD1 IGS mice (Charles River). For each stage, back tissue dorsal to rib cage at the level of forelimb was dissected out. Neural tube/spinal cord and dorsal root ganglion were removed wherever possible. For E15.5, epidermis and underlying dermis was removed before dissociating the tissue. Dissected tissues were washed several times in Hanks' Balanced Salt Solution (HBSS, Thermo Fisher Scientific, 14170112). Tissues were transferred to microfuge tube with 200μl of 2.5mg/ml Collagenase, (Type IV, Thermo Fisher Scientific, 17104019) and 0.05% Trypsine EDTA (Thermo Fisher Scientific, 25200-056) in PBS (Gibco, 14190), chopped into small pieces using scissors and incubated at 37°C for 15 minutes with intermittent shaking. Tissues were mechanically dissociated by triturating several times using wide-bore 1ml pipette. The resulting cell suspension was mixed with HBBS + 10% FBS, filtered through a 30μm cell strainer and spun at 300g for 5 minutes. To remove red blood cells, cell pellet was resuspended and incubated with RBC Lysis Solution (Qiagen, 158902) for 5 minutes at room temperature. Cells were washed with HBSS + 10% FBS for 2-3 times to remove debris. Final suspension was made in PBS + 0.1% BSA. Cell density was adjusted to 200,000/ml. For each stage, cells were collected from two littermate embryos. For E11.5-14.5 embryo, 3000 cells were encapsulated and sequenced from each embryo. For E15.5, 5000 cells were collected and sequenced from each embryo.

Encapsulation, sequencing and analysis

Single cells were encapsulated using inDrops technique as reported previously (Klein et al.). Cells were barcoded using v3 sequencing adapters and were sequenced on an Illumina NextSeq 500 using the NextSeq 75 High Output Kits using standard Illumina sequencing primers and 61 cycles for Read1, 14 cycles for Read2, 8 cycles each for IndexRead1 and IndexRead2. Sequence FASTQ files were processed according to indrops.py pipeline (available at github.com/indrops/indrops). Single cell transcriptomes were mapped to mouse (GRCm38/mm10) and human (GRCh38/hg19) reference transcriptomes. Samtools version 1.3.1, rsem version 1.3.0 and Bowtie version 1.2.2 was used with parameter –e 100.

A weighted histogram of transcript counts per cell barcode vs cell barcode abundance was used to identify transcripts originating from abundant cell barcodes. Only transcript counts originating from abundant cell barcodes were included in downstream analysis. Basic filtering parameters were used to exclude cells expressing <500 genes and genes expressed in less than 3 cells. The filtered counts were normalized by total number of counts for each biological sample. Top 1000 variable genes were identified according to Satija 2015. Cell doublets were identified using Scrublet and filtered out.[65] For each cell, fraction of counts due to mitochondrial genes was determined and cells with high fraction were filtered out. The cell cycle was scored as in Tirosh et al.[66] Each cell was given a cell cycle score based on the expression of G2/M and S phase markers. The cells not expressing the markers from G2/M and S phase were identified to be in G0/G1 stage. Source of variation between the libraries were regressed out using bkknn batch correction function.[67] Single cell data were projected into a low dimensional space by principal component analysis (PCA). UMAP[68] was used to embed the neighborhood graph. Cell clusters were identified using Leiden graph-clustering method.[69] Differentially expressed genes were identified by a Wilcoxon rank-sum test by comparing cells of each cluster with cells of all the other clusters.

Trackplot were made using each gene are plotted as a filled line plot where the y are the genes processed expression values and x is each of the cells.[70]

Stream: Stream pipeline was used to layout the trajectories inside each dataset.[25] Neural cells were removed from the dataset analyzed with stream as their developmental origin differ from the rest of the clusters.

Trajectory inference analysis was done using Cellrank.[71] Waddington-OT kernel[26] was used to infer the temporal couplings of cells from the different samples collected independently at various timepoints. Transition matrices were calculated to show the amount of mass transported from a cell type to another from a start and an end point.

Single cell RNA sequencing data from mouse E18 perivascular adipose tissue (pVAT) described in Angueira et al.[27] was processed through the same processing pipeline as described above. Cell state predictions on single cell clusters from pVAT described in Angueira et al.[27] were made using a kNN-classifier trained on our E13.5-E15.5 mouse single cell clusters.[23]

QUANTIFICATION AND STATISTICAL ANALYSIS

Statistical analyses were performed using GraphPad Prism (v8.1.1). Statistical parameters such as the value of n, mean, standard deviation (SD), p values, and the statistical tests used are reported in the figure legends. For hiPSC differentiation experiments, the "n" refers to the number of independent hiPSC differentiation experiments analyzed. In mouse embryo studies, "n" indicates the number of embryos from which samples were obtained. In human primary tissue studies, "n" indicates the number of randomly selected imaging regions from each specimen. All bar graphs and line graphs are displayed as mean ± SD. Paired or unpaired student's t-tests were used for two-sample comparisons.